Applied Numerical Mathematics 133 (2018) 2–24

Contents lists available at ScienceDirect

Applied Numerical Mathematics

www.elsevier.com/locate/apnum

A stabilized finite volume element method for a coupled Stokes–Darcy problem ☆

Rui Li [a], Jian Li [b,c], Xiaoming He [d,*], Zhangxin Chen [a,e]

[a] School of Mathematics and Statistics, Xi'an Jiaotong University, Xi'an, 710049, China
[b] Department of Mathematics, School of Arts and Sciences, Shaanxi University of Science and Technology, Xi'an 710021, China
[c] Department of Mathematics, Baoji University of Arts and Sciences, Baoji, 721007, China
[d] Department of Mathematics and Statistics, Missouri University of Science and Technology, Rolla, MO 65409, United States
[e] Department of Chemical & Petroleum Engineering, Schulich School of Engineering, University of Calgary, 2500 University Drive N. W., Calgary, Alberta T2N 1N4, Canada

ARTICLE INFO

Article history:
Available online 29 September 2017

Keywords:
Coupled Stokes–Darcy flow
Finite volume element method
Stability
Beavers–Joseph–Saffman–Jones condition

ABSTRACT

In this paper, we present a stabilized finite volume element method with the conforming finite element triples P_1–P_0–P_1 and P_1–P_1–P_1 for approximating the velocity, pressure, and hydraulic head of a coupled Stokes–Darcy problem. The proposed method is convenient to implement, computationally efficient, mass conserving, optimally accurate, and able to handle complex geometries; therefore, this method has great potential to be useful for realistic problems involving coupled free flow and porous media flow. To offset the lack of the inf-sup condition of the P_1–P_0 and P_1–P_1 elements for the Stokes equation, a parameter free stabilization term is added to the discrete formulation. Stability and optimal error estimates are proved based on a bridge built up between the finite volume element method and the finite element method. An element level implementation of the stabilization term is discussed so that an existing code package can be conveniently modified to handle the stabilization procedures. A series of numerical experiments are provided to illustrate the above features of the proposed method, the theoretical results, and the realistic applications.

1. Introduction

The conforming finite volume element method (FVEM) is a highly effective numerical method for partial differential equations, and therefore it has been extensively studied and widely applied to different types of problems, see [5,9,10,19,20,22,23,25,27,49,57,63,74,76] and references therein. The method combines the strengths of the finite volume and finite element methods. Specifically, as in the finite volume method, the FVEM is based on local conservation of mass, momentum, or energy. Also, as in the finite element method, the FVEM can easily deal with complicated geometries while also obtaining the optimal accuracy expected from the polynomials utilized for the finite element basis functions.

We consider the Stokes–Darcy model for coupling fluid flow in conduits with porous media flow. This type of coupled flow is often involved in many applications, such as subsurface flow problems [14,18,30,47,55], industrial filtrations [44],

☆ This work is partially supported by NSF grant DMS-1418624, NSFC (Nos. 11371031, 11771259), and Foundation CMG in Xi'an Jiaotong University.
* Corresponding author.
E-mail addresses: liruixjtu@163.com (R. Li), jiaaanli@gmail.com (J. Li), hex@mst.edu (X. He), zhachen@ucalgary.ca (Z. Chen).

https://doi.org/10.1016/j.apnum.2017.09.013
0168-9274/

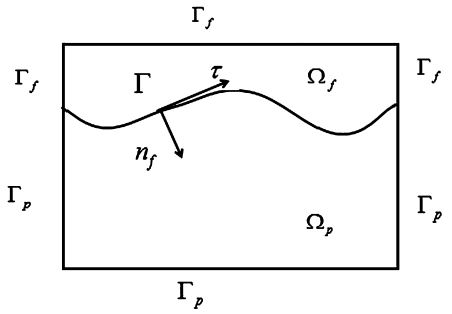

Fig. 1. A sketch of the porous medium domain Ω_p, fluid domain Ω_f and interface Γ.

and flow in vuggy porous media [2]. The model consists of Stokes equations to govern the flow in conduits, Darcy's law to govern the flow in porous media, and three interface conditions to couple these two constituent models together.

Due to the complexity of this model, many methods have been developed to numerically solve the Stokes–Darcy system, such as coupled finite element methods [12,13,48,52,58,62], domain decomposition methods (DDMs) [16,17,29,31,43,73], Lagrange multiplier methods [3,37,38,54], multigrid methods [1,11,64,80], discontinuous Galerkin methods [40,51,61,67,68], discontinuous finite volume element method [59,75], mortar finite element methods [32,35,41], least square methods [33,46,56,66,72], partitioned time stepping methods [53,65,70], and boundary integral methods [7,8,71], hybridizable discontinuous Galerkin methods [36], and weak Galerkin methods [24,60]. We consider the conforming FVEM, and show that it is able to conveniently and efficiently solve sophisticated coupled flow problems while conserving mass and obtaining optimal convergence rates.

Practitioners often prefer to utilize low-order finite elements, such as P_0 and P_1 elements, since they are simple to implement and can provide enough accuracy for many applications. However, the P_1–P_0 and P_1–P_1 finite element pairs are not stable for the Stokes equations since they do not satisfy the inf-sup condition [21,39,42]. We use the idea in [6] to develop a stabilized finite volume element method for applying the low-order finite element triples P_1–P_1–P_1 and P_1–P_0–P_1 to solve the Stokes–Darcy system, where P_1 elements are applied to the second order primary formulation of the Darcy's law. Implementation of the stabilized scheme relies on projection operators, which only need the standard nodal data structures and can be conveniently evaluated at the element level.

One might think that the development and analysis of a new method for the Stokes–Darcy model should simply follow by combining available approaches for the Stokes and Darcy problems; however, this is not the case. As we can see from the above existing literature for the Stokes–Darcy model, this combination approach only works partially since significant difficulties and technical issues often arise from the interface conditions. In our work, a major difficulty in the analysis is to bound the interface integrals arising from the interface conditions. To deal with this, we extend the equivalence relationship between the stabilized finite volume element method and a stabilized finite element method in [77] to the coupled Stokes–Darcy problem. The key for proving the equivalence is to handle the interface conditions appropriately. Once this relationship is established, we utilize existing theoretical results for the stabilized finite element method to analyze the stabilized finite volume element method for the Stokes–Darcy model, and we obtain optimal convergence rates in both H^1 and L^2 norms.

Based on the work in [6], we provide implementation techniques for the projection operators Π_h^0 and Π_h^1 which are the keys for the stabilization. We discuss about Π_h^0 based on two local quadrature rules and Π_h^1 based on Clement-like interpolation, both of which can be evaluated locally at the element level using standard finite element techniques. As a result, an existing code package can be easily modified to handle the stabilization procedures. Finally, the theoretical results and the features of the proposed method will be demonstrated by computational results, such as the optimal accuracy orders, mass conservation, capability to conveniently deal with complicated geometries, and applicability to realistic parameters and problems.

The paper is organized as follows: in section 2, we briefly introduce the Stokes–Darcy model and its weak formulation; in sections 3 and 4, the stabilized finite volume element method is proposed and analyzed; in section 5, some implementation issues are discussed and a series of numerical experiments are provided; finally, conclusions are presented in section 6.

Throughout the paper, the letter C denotes a positive constant independent of the mesh size and may indicate different values in different places.

2. A Coupled Stokes–Darcy problem

We consider a coupled Stokes–Darcy model in a bounded domain $\Omega \subset \mathbb{R}^2$, consisting of a fluid region Ω_f and a porous medium region Ω_p, with interface $\Gamma = \partial\Omega_f \bigcap \partial\Omega_p$. Both Ω_f and Ω_p have Lipschitz continuous boundaries. Define $\Gamma_i = \partial\Omega_i \backslash \Gamma$ for $i = f, p$. Moreover, let $\mathbf{n}_f$ denote the unit normal vector of Γ pointing from Ω_f to Ω_p and let τ denote the corresponding unit tangential vector; see Fig. 1.

In Ω_f, the fluid flow is assumed to be governed by the Stokes equations:

$$\begin{cases} -\nabla \cdot \mathbf{T}(\mathbf{u}_f, p_f) = \mathbf{f}_f & \text{in} \quad \Omega_f, \\ \nabla \cdot \mathbf{u}_f = 0 & \text{in} \quad \Omega_f, \end{cases} \tag{1}$$

where $\mathbf{T}(\mathbf{u}_f, p_f) = -p_f \mathbf{I} + 2\nu \mathbb{D}(\mathbf{u}_f)$ is the stress tensor, $\mathbb{D}(\mathbf{u}_f) = \frac{1}{2}(\nabla \mathbf{u}_f + (\nabla \mathbf{u}_f)^T)$ is the velocity deformation tensor, ν is the kinetic viscosity, $\mathbf{u}_f$ denotes the fluid velocity, p_f denotes the kinematic pressure, and $\mathbf{f}_f$ denotes a general body force term that includes gravitational acceleration.

In Ω_p, the flow is governed by Darcy's law:

$$\begin{cases} \nabla \cdot \mathbf{u}_p = f_p & \text{in} \quad \Omega_p, \\ \mathbf{u}_p = -\mathbb{K} \nabla \phi_p & \text{in} \quad \Omega_p, \end{cases} \tag{2}$$

where $\mathbf{u}_p$ is the specific discharge rate in the porous medium, $\mathbb{K}$ is the hydraulic conductivity tensor, f_p is a sink/source term, and ϕ_p is the hydraulic head. Furthermore, ϕ_p is linearly related to the dynamic pressure p_p: $\phi_p = z + \frac{p_p}{\rho g}$, where ρ is the density, z is the relative depth from an arbitrary fixed reference height, and g is the gravitational acceleration. By (2), we obtain

$$-\nabla \cdot (\mathbb{K} \nabla \phi_p) = f_p \quad \text{in} \quad \Omega_p. \tag{3}$$

The key part for this coupled model is the interface conditions that describe how different types of flow interact at the fluid/porous medium interface Γ:

$$\mathbf{u}_f \cdot \mathbf{n}_f = \mathbf{u}_p \cdot \mathbf{n}_f \quad \text{on} \quad \Gamma, \tag{4}$$

$$-\mathbf{n}_f \cdot (\mathbf{T}(\mathbf{u}_f, p_f) \cdot \mathbf{n}_f) = g(\phi_p - z) \quad \text{on} \quad \Gamma, \tag{5}$$

$$-\tau \cdot (\mathbf{T}(\mathbf{u}_f, p_f) \cdot \mathbf{n}_f) = \frac{\alpha \nu \sqrt{d}}{\sqrt{trace(\mathbf{\Pi})}} \tau \cdot \mathbf{u}_f \quad \text{on} \quad \Gamma, \tag{6}$$

where d denotes the space dimension, α is the Beavers–Joseph [4] constant depending on the properties of the porous medium, and the permeability $\mathbf{\Pi} = \frac{\mathbb{K}\nu}{g}$. Let $\mathbf{P}_\tau$ be the projection onto the tangent space on Γ defined as $\mathbf{P}_\tau(\mathbf{u}_f) = (\mathbf{u}_f \cdot \tau) \cdot \tau$. The last equation of (6) is called the Beavers–Joseph–Saffman–Jones condition [50,69].

For simplicity, we assume that the hydraulic head ϕ_p and the fluid velocity $\mathbf{u}_f$ satisfy homogeneous Dirichlet boundary conditions except on Γ; i.e., $\phi_p = 0$ on Γ_p and $\mathbf{u}_f = \mathbf{0}$ on Γ_f. We also assume that $z = 0$ and $\mathbb{K} = k\mathbb{I}$ where $\mathbb{I}$ is the identity matrix.

The Sobolev space $H^s(D) = W^{2,s}(D)$ is defined in the usual way for $D = \Omega_f$ or Ω_p with the norm and seminorm $\|\cdot\|_{s,D}$ and $|\cdot|_{s,D}$, respectively. We also define the spaces

$$\begin{aligned} \mathbf{X}_f &= \{\mathbf{v} \in [H^1(\Omega_f)]^2 \quad | \quad \mathbf{v} = 0 \quad \text{on} \quad \partial\Omega_f \setminus \Gamma\}, \\ X_p &= \{\psi \in H^1(\Omega_p) \quad | \quad \psi = 0 \quad \text{on} \quad \partial\Omega_p \setminus \Gamma\}, \\ Q_f &= \{q \in L^2(\Omega_f)\}. \end{aligned}$$

In the rest of paper we use $\mathbf{u}, \phi$, and p to replace $\mathbf{u}_f, \phi_p$, and p_f for simpler notations in the analysis, in particular, we use the following notations for the norms:

$$\begin{aligned} \|\mathbf{u}\|_0 &:= \|\mathbf{u}\|_{L^2(\Omega_f)}, \qquad \|\mathbf{u}\|_1 := \|\mathbf{u}\|_{\mathbf{X}_f(\Omega_f)}, \\ \|\phi\|_0 &:= \|\phi\|_{L^2(\Omega_p)}, \qquad \|\phi\|_1 := \|\phi\|_{X_p(\Omega_p)}, \\ \|p\|_0 &:= \|p\|_{L^2(\Omega_f)}. \end{aligned}$$

For a domain D ($D = \Omega_f$ or Ω_p), let $(\cdot,\cdot)_D$ denote the L^2 inner product on D and $\langle \cdot, \cdot \rangle$ denote the L^2 inner product on the interface Γ or the duality pairing between $(H_{00}^{1/2}(\Gamma))'$ and $H_{00}^{1/2}(\Gamma)$.

With these notation, a weak formulation of the coupled Stokes–Darcy problem is given as follows [28,54]: Find $(\mathbf{u}, p) \in \mathbf{X}_f \times Q_f$ and $\phi \in X_p$ such that

$$\begin{cases} a_f(\mathbf{u}, \mathbf{v}) - b_f(\mathbf{v}, p) + g a_p(\phi, \psi) + g\langle \phi, \mathbf{v} \cdot \mathbf{n}_f \rangle_\Gamma - g\langle \mathbf{u} \cdot \mathbf{n}_f, \psi \rangle_\Gamma + \frac{\alpha \nu \sqrt{d}}{\sqrt{trace(\mathbf{\Pi})}} \langle \mathbf{P}_\tau(\mathbf{u}), \mathbf{P}_\tau(\mathbf{v}) \rangle_\Gamma \\ = (\mathbf{f}_f, \mathbf{v})_{\Omega_f} + g(f_p, \psi)_{\Omega_p}, \qquad \forall \mathbf{v} \in \mathbf{X}_f, \ \psi \in X_p, \\ b_f(\mathbf{u}, q) = 0, \qquad \forall q \in Q_f, \end{cases} \tag{7}$$

where the bilinear forms are defined as

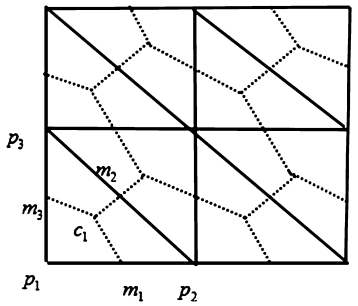

Fig. 2. Conforming triangulation and its dual.

$$a_f(\mathbf{u},\mathbf{v}) = 2\nu(\mathbb{D}(\mathbf{u}),\mathbb{D}(\mathbf{v}))_{\Omega_f},$$
$$a_p(\phi,\psi) = (k\nabla\phi,\nabla\psi)_{\Omega_p},$$
$$b_f(\mathbf{v},q) = (\nabla\cdot\mathbf{v},q)_{\Omega_f}.$$

Define

$$B((\mathbf{u},p,\phi),(\mathbf{v},q,\psi)) = a_f(\mathbf{u},\mathbf{v}) + ga_p(\phi,\psi) + g\langle\phi,\mathbf{v}\cdot\mathbf{n}_f\rangle - g\langle\mathbf{u}\cdot\mathbf{n}_f,\psi\rangle + \frac{\alpha\nu\sqrt{d}}{\sqrt{trace(\mathbf{\Pi})}}\langle\mathbf{P}_\tau(\mathbf{u}),\mathbf{P}_\tau(\mathbf{v})\rangle - b_f(\mathbf{v},p) + b_f(\mathbf{u},q). \tag{8}$$

Then, we can rewrite the weak formulation (7) as

$$B((\mathbf{u},p,\phi),(\mathbf{v},q,\psi)) = (\mathbf{f}_f,\mathbf{v})_{\Omega_f} + g(f_p,\psi)_{\Omega_p}, \quad \forall(\mathbf{v},q,\psi)\in\mathbf{X}_f\times Q_f\times X_p. \tag{9}$$

3. Stabilized finite volume element method

Let $\mathcal{T}_{h_i}(i=f,\,p)$ be a regular triangulation of Ω_i, where the mesh parameter $h_i = \max_{K\in\mathcal{T}_{h_i}}\mathrm{diam}(K)$. Let $\mathcal{N}_i$ be the set of all the nodal points associated with the partition $\mathcal{T}_{h_i}$, N_i be the total number of the nodes in $\mathcal{N}_i$. The dual partition $\mathcal{T}_{h_i}^*$ corresponding to the primal partition $\mathcal{T}_{h_i}$ is designed by connecting the barycentres of the triangles in $\mathcal{T}_{h_i}$ with the midpoints of their edges as shown in Fig. 2. For each nodal $p_j\in\mathcal{N}_i(j=1,2,\cdots,N_i)$, there exists a polygonal $K_j^*\in\mathcal{T}_{h_i}^*$ surrounding p_j. K_j^* is called box or control volume.

We define finite-dimensional subspaces of $\mathbf{X}_f$, Q_f and X_p as follows,

$$\mathbf{X}_{h_f} = \{\mathbf{v}\in C^0(\Omega_f)^2\cap\mathbf{X}_f : \mathbf{v}\,|_K\in[P_1(K)]^2,\quad \forall K\in\mathcal{T}_{h_f}\},$$
$$X_{h_p} = \{\psi\in C^0(\Omega_p)\cap X_p : \psi\,|_K\in P_1(K),\quad \forall K\in\mathcal{T}_{h_p}\},$$

$$Q_{h_f} \triangleq \begin{cases} Q_{h_f}^0 = \{q\in L^2(\Omega_f)\cap Q_f : q\,|_K\in P_0(K),\quad \forall\, K\in\mathcal{T}_{h_f}\},\\ Q_{h_f}^1 = \{q\in C^0(\Omega_f)\cap Q_f : q\,|_K\in P_1(K),\quad \forall\, K\in\mathcal{T}_{h_f}\}.\end{cases}$$

For the finite element spaces $\mathbf{X}_{h_f}\times Q_{h_f}\times X_{h_p}$, the following approximate properties hold: $\forall(\mathbf{v},q,\psi)\in[H^2(\Omega_f)]^2\times H^1(\Omega_f)\times H^2(\Omega_p)$, there exist approximations $I_h\mathbf{v}\in\mathbf{X}_{h_f}$, $J_h\psi\in X_{h_p}$ and $\rho_h q\in Q_{h_f}$ such that

$$\|\mathbf{v}-I_h\mathbf{v}\|_l \le Ch_f^{2-l}\|\mathbf{v}\|_2, \quad l=0,1, \tag{10}$$
$$\|\psi-J_h\psi\|_l \le Ch_p^{2-l}\|\psi\|_2, \quad l=0,1, \tag{11}$$
$$\|q-\rho_h q\|_0 \le Ch_f\|q\|_1, \tag{12}$$
$$\|I_h\mathbf{v}\|_1 \le C\|\mathbf{v}\|_1, \tag{13}$$
$$\|J_h\psi\|_1 \le C\|\psi\|_1, \tag{14}$$
$$\|\rho_h q\|_0 \le C\|q\|_0. \tag{15}$$

The test function spaces are defined by

$$\mathbf{X}_{h_f}^* = \{\mathbf{v}_h \in [L^2(\Omega_f)]^2 : \mathbf{v}_h|_{K_j^*} \in [P_0(K_j^*)]^2, \quad \forall K_j^* \in \mathcal{T}_{h_f}^*\},$$
$$X_{h_p}^* = \{\psi_h \in L^2(\Omega_p) : \psi_h|_{K_j^*} \in P_0(K_j^*), \quad \forall K_j^* \in \mathcal{T}_{h_p}^*\}.$$

Define interpolation operator $\Gamma_{h_f} : \mathbf{X}_{h_f} \to \mathbf{X}_{h_f}^*$ by

$$\Gamma_{h_f}\mathbf{v}_h(x) = \sum_{j=1}^{N_f} \mathbf{v}_h(p_j)\mathcal{X}_j(x), \quad \forall x \in \Omega_f, \forall \mathbf{v}_h \in \mathbf{X}_{h_f},$$

where

$$\mathcal{X}_j(x) = \begin{cases} 1 & \text{if } x \in K_j^* \in \mathcal{T}_{h_f}^*, \\ 0 & \text{otherwise,} \end{cases}$$

and interpolation operator $\Gamma_{h_p} : X_{h_p} \to X_{h_p}^*$ by

$$\Gamma_{h_p}\psi_h(x) = \sum_{j=1}^{N_p} \psi_h(p_j)\mathcal{X}_j(x), \quad \forall x \in \Omega_p, \forall \psi_h \in X_{h_p},$$

where

$$\mathcal{X}_j(x) = \begin{cases} 1 & \text{if } x \in K_j^* \in \mathcal{T}_{h_p}^*, \\ 0 & \text{otherwise.} \end{cases}$$

For each nodal $p_n \in \mathcal{N}_i (n = 1, 2, \cdots, N_i;\ i = f,\ p)$, we have

$$\Gamma_{h_p}\psi_h(p_n) = \sum_{j=1}^{N_p} \psi_h(p_j)\mathcal{X}_j(p_n) = \psi_h(p_n), \tag{16}$$

$$\Gamma_{h_f}\mathbf{v}_h(p_n) = \sum_{j=1}^{N_f} \mathbf{v}_h(p_j)\mathcal{X}_j(p_n) = \mathbf{v}_h(p_n). \tag{17}$$

The mappings Γ_{h_f} and Γ_{h_p} satisfy the following properties [57,77]: if $\mathbf{v}_h \in \mathbf{X}_{h_f}, \psi_h \in X_{h_p}$, then

$$\int_{K \in \mathcal{T}_{h_f}} (\mathbf{v}_h - \Gamma_{h_f}\mathbf{v}_h)dx = 0, \quad \int_{K \in \mathcal{T}_{h_p}} (\psi_h - \Gamma_{h_p}\psi_h)dx = 0, \tag{18}$$

$$\|\mathbf{v}_h - \Gamma_{h_f}\mathbf{v}_h\|_0 \le Ch\|\mathbf{v}_h\|_1, \quad \|\psi_h - \Gamma_{h_p}\psi_h\|_0 \le Ch\|\psi_h\|_1. \tag{19}$$

To obtain the discrete formulation, perform the following steps: multiply the first equation in (1) by $\Gamma_{h_f}\mathbf{v}_h \in \mathbf{X}_{h_f}^*$ and integrate over each dual element $K_j^* \in \mathcal{T}_{h_f}^* (j = 1, 2, \cdots, N_f)$; multiply the second equation in (1) by $q_h \in Q_{h_f}$ and integrate over each primal element $K \in \mathcal{T}_{h_f}$; multiply equation (3) by $\Gamma_{h_p}\psi_h \in X_{h_p}^*$ and integrate over each dual element $K_j^* \in \mathcal{T}_{h_p}^* (j = 1, 2, \cdots, N_p)$; apply integration by parts and interface condition (4)–(6); and add the above equations. The resulting discrete formulation is to find $(\mathbf{u}_h^*, p_h^*, \phi_h^*) \in (\mathbf{X}_{h_f}, Q_{h_f}, X_{h_p})$ such that

$$\begin{cases} \tilde{a}_f(\mathbf{u}_h^*, \Gamma_{h_f}\mathbf{v}_h) + \tilde{b}_f(\Gamma_{h_f}\mathbf{v}_h, p_h^*) + g\tilde{a}_p(\phi_h^*, \Gamma_{h_p}\psi_h) + g\langle\phi_h^*, \Gamma_{h_f}\mathbf{v}_h \cdot \mathbf{n}_f\rangle_\Gamma \\ -g\langle\mathbf{u}_h^* \cdot \mathbf{n}_f, \Gamma_{h_p}\psi_h\rangle_\Gamma + \frac{\alpha\nu\sqrt{d}}{\sqrt{trace(\mathbf{\Pi})}}\langle\mathbf{P}_\tau(\mathbf{u}_h^*), \mathbf{P}_\tau(\Gamma_{h_f}\mathbf{v}_h)\rangle_\Gamma \\ = (\mathbf{f}_f, \Gamma_{h_f}\mathbf{v}_h) + g(f_p, \Gamma_{h_p}\psi_h), \qquad \forall \mathbf{v}_h \in \mathbf{X}_{h_f},\ \psi_h \in X_{h_p}, \\ b_f(\mathbf{u}_h^*, q_h) = 0, \qquad \forall q_h \in Q_{h_f}, \end{cases} \tag{20}$$

where bilinear and linear forms are defined as follows:

$$\tilde{a}_f(\mathbf{u}_h^*, \Gamma_{h_f}\mathbf{v}_h) = -\sum_{j=1}^{N_f} \mathbf{v}_h(p_j) \cdot \int_{\partial K_j^* \bigcap \Omega_f \setminus \Gamma} 2\nu\mathbb{D}(\mathbf{u}_h^*) \cdot \mathbf{n}ds, \quad \forall \mathbf{u}_h^*, \mathbf{v}_h \in \mathbf{X}_{h_f},$$

$$\tilde{b}_f(\Gamma_{h_f}\mathbf{v}_h, p_h^*) = \sum_{j=1}^{N_f} \mathbf{v}_h(p_j) \cdot \int_{\partial K_j^* \bigcap \Omega_f \setminus \Gamma} p_h^*\mathbf{n}ds, \quad \forall \mathbf{v}_h \in \mathbf{X}_{h_f}, p_h^* \in Q_{h_f},$$

$$\tilde{a}_p(\phi_h^*, \Gamma_{h_p}\psi_h) = -\sum_{j=1}^{N_p}\psi_h(p_j)\cdot\int\limits_{\partial K_j^*\bigcap\Omega_p\backslash\Gamma} k\nabla\phi_h^*\cdot\mathbf{n}ds,\quad \forall\phi_h^*,\psi_h\in X_{h_p},$$

$$\langle\phi_h^*, \Gamma_{h_f}\mathbf{v}_h\cdot\mathbf{n}_f\rangle_\Gamma = \sum_{j=1}^{N_f}\mathbf{v}_h(p_j)\cdot\int\limits_{\partial K_j^*\bigcap\Omega_f\bigcap\Gamma}\phi_h^*\mathbf{n}_f ds,\quad \forall\phi_h^*\in X_{h_p},\mathbf{v}_h\in\mathbf{X}_{h_f},$$

$$\langle\mathbf{u}_h^*\cdot\mathbf{n}_f, \Gamma_{h_p}\psi_h\rangle_\Gamma = \sum_{j=1}^{N_p}\psi_h(p_j)\cdot\int\limits_{\partial K_j^*\bigcap\Omega_p\bigcap\Gamma}\mathbf{u}_h^*\cdot\mathbf{n}_f ds,\quad \forall\psi_h\in X_{h_p},\mathbf{u}_h^*\in\mathbf{X}_{h_f},$$

$$\langle\mathbf{P}_\tau(\mathbf{u}_h^*), \mathbf{P}_\tau(\Gamma_{h_f}\mathbf{v}_h)\rangle_\Gamma = \sum_{j=1}^{N_f}\mathbf{v}_h(p_j)\cdot\int\limits_{\partial K_j^*\bigcap\Omega_f\bigcap\Gamma}(\mathbf{u}_h^*\cdot\tau)\cdot\tau ds,\quad \forall\mathbf{u}_h^*,\mathbf{v}_h\in\mathbf{X}_{h_f},$$

$$(\mathbf{f}_f, \Gamma_{h_f}\mathbf{v}_h) = \sum_{j=1}^{N_f}\mathbf{v}_h(p_j)\cdot\int\limits_{K_j^*\bigcap\Omega_f}\mathbf{f}_f dx,\quad \forall\mathbf{v}_h\in\mathbf{X}_{h_f},$$

$$(f_p, \Gamma_{h_p}\psi_h) = \sum_{j=1}^{N_p}\psi_h(p_j)\int\limits_{K_j^*\bigcap\Omega_p} f_p dx,\quad \forall\psi_h\in X_{h_f},$$

where $\mathbf{n}$ is the unit normal outward to ∂K_j^*. The choice of the low-order FE pairs results in an ill-posed discrete problem due to the instability arising from violating the inf-sup condition. One way to resolve this problem is to add a stabilization term $G(p_h, q_h)$ [6,79], which is defined by

$$G(p_h, q_h) = ((I-\Pi_h)p_h, (I-\Pi_h)q_h), \tag{21}$$

in the bilinear form. Here the projection operator Π_h is defined as

$$\Pi_h = \begin{cases}\Pi_h^0: & L^2(\Omega_f)\to Q_{h_f}^0,\\ \Pi_h^1: & L^2(\Omega_f)\to Q_{h_f}^1.\end{cases} \tag{22}$$

The projection operators Π_h^0 or Π_h^1 are designed in [6], and mainly act on the pressure as a stabilization. In [79], Π_h^0 and Π_h^1 are constructed based on two local quadrature rules and a Clement-like interpolation respectively, which are easy to compute locally. In this paper, Π_h^0 will be used to stabilize the P_1–P_1–P_1 finite element triple and Π_h^1 will be used to stabilize the P_1–P_0–P_1 finite element triple. Recall that Π_h satisfies the following properties [6,57]

$$||\Pi_h p||_0 \le C||p||_0,\quad \forall p\in Q_f, \tag{23}$$

$$||\Pi_h p - p||_0 \le Ch||p||_1,\quad \forall p\in H^1(\Omega)\cap Q_f. \tag{24}$$

Now we define the stabilized FVEM approximation of problem (1)–(6): find $(\mathbf{u}_h^*, p_h^*, \phi_h^*)\in(\mathbf{X}_{h_f}, Q_{h_f}, X_{h_p})$ such that for all $(\mathbf{v}_h, q_h, \psi_h)\in(\mathbf{X}_{h_f}, Q_{h_f}, X_{h_p})$,

$$\begin{cases}\tilde{a}_f(\mathbf{u}_h^*, \Gamma_{h_f}\mathbf{v}_h) + \tilde{b}_f(\Gamma_{h_f}\mathbf{v}_h, p_h^*) + g\tilde{a}_p(\phi_h^*, \Gamma_{h_p}\psi_h) + g\langle\phi_h^*, \Gamma_{h_f}\mathbf{v}_h\cdot\mathbf{n}_f\rangle_\Gamma\\ -g\langle\mathbf{u}_h^*\cdot\mathbf{n}_f, \Gamma_{h_p}\psi_h\rangle_\Gamma + \frac{\alpha\nu\sqrt{d}}{\sqrt{trace(\mathbf{\Pi})}}\langle\mathbf{P}_\tau(\mathbf{u}_h^*), \mathbf{P}_\tau(\Gamma_{h_f}\mathbf{v}_h)\rangle_\Gamma\\ = (\mathbf{f}_f, \Gamma_{h_f}\mathbf{v}_h) + g(f_p, \Gamma_{h_p}\psi_h),\qquad \forall\mathbf{v}_h\in\mathbf{X}_{h_f},\ \psi_h\in X_{h_p},\\ b_f(\mathbf{u}_h^*, q_h) + G(p_h^*, q_h) = 0,\qquad \forall q_h\in Q_{h_f}.\end{cases} \tag{25}$$

Define the bilinear form

$$\begin{aligned}&\tilde{B}_h^*((\mathbf{u}_h^*, p_h^*, \phi_h^*), (\mathbf{v}_h, q_h, \psi_h))\\ &= \tilde{a}_f(\mathbf{u}_h^*, \Gamma_{h_f}\mathbf{v}_h) + \tilde{b}_f(\Gamma_{h_f}\mathbf{v}_h, p_h^*) + g\tilde{a}_p(\phi_h^*, \Gamma_{h_p}\psi_h) + g\langle\phi_h^*, \Gamma_{h_f}\mathbf{v}_h\cdot\mathbf{n}_f\rangle_\Gamma\\ &\quad - g\langle\mathbf{u}_h^*\cdot\mathbf{n}_f, \Gamma_{h_p}\psi_h\rangle_\Gamma + \frac{\alpha\nu\sqrt{d}}{\sqrt{trace(\mathbf{\Pi})}}\langle\mathbf{P}_\tau(\mathbf{u}_h^*), \mathbf{P}_\tau(\Gamma_{h_f}\mathbf{v}_h)\rangle_\Gamma + b_f(\mathbf{u}_h^*, q_h) + G(p_h^*, q_h).\end{aligned} \tag{26}$$

Then the above scheme can be rewritten as:

$$\tilde{B}_h^*((\mathbf{u}_h^*, p_h^*, \phi_h^*), (\mathbf{v}_h, q_h, \psi_h)) = (\mathbf{f}_f, \Gamma_{h_f}\mathbf{v}_h) + g(f_p, \Gamma_{h_p}\psi_h), \quad \forall (\mathbf{v}_h, q_h, \psi_h) \in (\mathbf{X}_{h_f}, Q_{h_f}, X_{h_p}). \tag{27}$$

4. Error estimates

The goal of this section is to present the error analysis for the stabilized finite volume element discretization scheme (27). The main idea is to build up a critical equivalence relationship between the stabilized finite volume element method and the stabilized finite element method [77]. Therefore, we first recall the analysis results for the stabilized finite element method and then prove the equivalence before we prove the convergence of the stabilized finite volume element method.

4.1. Stabilized finite element approximation

In this article, we choose P_1–P_1 and P_1–P_0 pairs for the finite element spaces $\mathbf{X}_{h_f} \times Q_{h_f}$. Since the two pairs do not satisfy the discrete inf-sup condition, we recall the following stabilized finite element method [58]: find $(\mathbf{u}_h, p_h, \phi_h) \in (\mathbf{X}_{h_f}, Q_{h_f}, X_{h_p})$ such that for all $(\mathbf{v}_h, q_h, \psi_h) \in (\mathbf{X}_{h_f}, Q_{h_f}, X_{h_p})$,

$$\tilde{B}_h((\mathbf{u}_h, p_h, \phi_h), (\mathbf{v}_h, q_h, \psi_h)) = (\mathbf{f}_f, \mathbf{v}_h)_{\Omega_f} + g(f_p, \psi_h)_{\Omega_p}, \tag{28}$$

where

$$\begin{aligned}
&\tilde{B}_h((\mathbf{u}_h, p_h, \phi_h), (\mathbf{v}_h, q_h, \psi_h)) \\
&= a_f(\mathbf{u}_h, \mathbf{v}_h) + g a_p(\phi_h, \psi_h) + g\langle \phi_h, \mathbf{v}_h \cdot \mathbf{n}_f\rangle - g\langle \mathbf{u}_h \cdot \mathbf{n}_f, \psi_h\rangle \\
&\quad + \frac{\alpha \nu \sqrt{d}}{\sqrt{trace(\mathbf{\Pi})}} \langle \mathbf{P}_\tau(\mathbf{u}_h), \mathbf{P}_\tau(\mathbf{v}_h)\rangle - b_f(\mathbf{v}_h, p_h) + b_f(\mathbf{u}_h, q_h) + G(p_h, q_h).
\end{aligned} \tag{29}$$

For P_1–P_1–P_1 finite element scheme, the bilinear form $\tilde{B}_h((\cdot,\cdot,\cdot),(\cdot,\cdot,\cdot))$ satisfies the following continuity and weak coercivity properties [58]:

Theorem 4.1.1. *The bilinear form $\tilde{B}_h((\mathbf{u}_h, p_h, \phi_h), (\mathbf{v}_h, q_h, \psi_h))$ satisfies the continuity property*

$$\tilde{B}_h((\mathbf{u}_h, p_h, \phi_h), (\mathbf{v}_h, q_h, \psi_h)) \le C(\|\mathbf{u}_h\|_1 + \|p_h\|_0 + \|\phi_h\|_1)(\|\mathbf{v}_h\|_1 + \|q_h\|_0 + \|\psi_h\|_1), \tag{30}$$

and the coercivity property

$$\sup_{0 \neq (\mathbf{v}_h, q_h, \psi_h) \in (\mathbf{X}_{h_f}, Q_{h_f}, X_{h_p})} \frac{|\tilde{B}_h((\mathbf{u}_h, p_h, \phi_h), (\mathbf{v}_h, q_h, \psi_h))|}{(\|\mathbf{v}_h\|_1^2 + \|q_h\|_0^2 + \|\psi_h\|_1^2)^{\frac{1}{2}}} \ge \beta(\|\mathbf{u}_h\|_1^2 + \|p_h\|_0^2 + \|\phi_h\|_1^2)^{\frac{1}{2}}, \tag{31}$$

where β is a positive constant depending only on the domain. Moreover, the optimal error estimate for the finite element solution $(\mathbf{u}_h, p_h, \phi_h)$ holds for sufficiently small h.

Theorem 4.1.2. *Let $(\mathbf{u}, p, \phi)$ and $(\mathbf{u}_h, p_h, \phi_h)$ be the solutions of (9) and (28), respectively. Then we have*

$$\|\mathbf{u} - \mathbf{u}_h\|_1 + \|\phi - \phi_h\|_1 + \|p - p_h\|_0 \le Ch(\|\mathbf{u}\|_2 + \|\phi\|_2 + \|p\|_1). \tag{32}$$

Moreover, the L^2-error estimate is obtained:

$$\|\mathbf{u} - \mathbf{u}_h\|_0 + \|\phi - \phi_h\|_0 \le Ch^2(\|\mathbf{u}\|_2 + \|\phi\|_2 + \|p\|_1). \tag{33}$$

Remark 4.1. For the P_1–P_0–P_1 finite element scheme, one can show that the bilinear form $\tilde{B}_h((\cdot,\cdot,\cdot),(\cdot,\cdot,\cdot))$ also satisfies (30)–(33) by using the same arguments in [58] for the proof of Theorem 4.1.1 and 4.1.2.

4.2. Equivalence between the stabilized finite volume element method and the stabilized finite element method

In this subsection, we establish the equivalence relationship between the stabilized finite volume element and stabilized finite element approximations for the coupled steady Stokes–Darcy problem. This relationship will play a key role in the error estimation of the next subsection.

For a $K \in \mathcal{T}_{h_i}$, let $\mathfrak{R}_{j+1}$ $(j = 1, 2, 3)$ denote the quadrangle $cm_j q_{j+1} m_{j+1}$ as illustrated in Fig. 3 where we consider the index $j+3$ to be the same as the index j. In order to prove the final equivalence relationship, we need to analyze the main terms in the finite volume element formulation one by one in the following four lemmas.

Lemma 4.2.1. *Let $(\mathbf{u}_h^*, p_h^*, \phi_h^*) \in (\mathbf{X}_{h_f}, Q_{h_f}, X_{h_p})$ be the solution of (27). For all $(\mathbf{v}_h, q_h, \psi_h) \in (\mathbf{X}_{h_f}, Q_{h_f}, X_{h_p})$, we have*

$$\tilde{a}_p(\phi_h^*, \Gamma_{h_p}\psi_h) = \sum_{K \in \mathcal{T}_{h_p}} (k\nabla\phi_h^*, \nabla\psi_h)_K + \int_\Gamma (\mathbf{u}_h^* \cdot \mathbf{n}_f)(\Gamma_{h_p}\psi_h - \psi_h) ds.$$

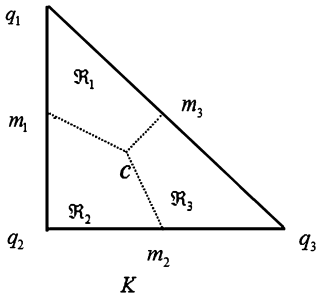

Fig. 3. A sketch of one element K.

Proof. For all ϕ_h^*, $\psi_h \in X_{h_p}$, we can easily see that $\Delta\phi_h^* = 0$, $\nabla(\psi_h(q_{j+1})) = 0$ on each element and $\frac{\partial\phi_h^*}{\partial\mathbf{n}}$ is a constant on $\partial K \setminus \Gamma$, $\forall\ K \in \mathcal{T}_{h_p}$. We also recall the following identity [77]:

$$\int\limits_{q_j m_j \bigcap \Omega_p \setminus \Gamma} \psi_h(q_j) ds + \int\limits_{m_j q_{j+1} \bigcap \Omega_p \setminus \Gamma} \psi_h(q_{j+1}) ds = \int\limits_{q_j q_{j+1} \bigcap \Omega_p \setminus \Gamma} \psi_h ds. \tag{34}$$

Then by using these conclusions together with Green's formula, (4), and (16), we get

$$\begin{aligned}
&\tilde{a}_p(\phi_h^*, \Gamma_{h_p}\psi_h) \\
&= -\sum_{n=1}^{N_p} \psi_h(p_n) \int\limits_{\partial K_n^* \bigcap \Omega_p \setminus \Gamma} k\frac{\partial\phi_h^*}{\partial\mathbf{n}} ds \\
&= -\sum_{K\in\mathcal{T}_{h_p}} \sum_{j=1}^{3} \psi_h(q_{j+1}) \int\limits_{m_{j+1} c m_j} k\frac{\partial\phi_h^*}{\partial\mathbf{n}} ds \\
&= \sum_{K\in\mathcal{T}_{h_p}} \sum_{j=1}^{3} \int\limits_{m_j q_{j+1} m_{j+1}} k\frac{\partial\phi_h^*}{\partial\mathbf{n}} \psi_h(q_{j+1}) ds - \sum_{K\in\mathcal{T}_{h_p}} \sum_{j=1}^{3} (k\Delta\phi_h^*, \psi_h(q_{j+1}))_{\mathfrak{R}_{j+1}} \\
&\quad - \sum_{K\in\mathcal{T}_{h_p}} \sum_{j=1}^{3} (k\nabla\phi_h^*, \nabla(\psi_h(q_{j+1})))_{\mathfrak{R}_{j+1}} \\
&= \sum_{K\in\mathcal{T}_{h_p}} \sum_{j=1}^{3} \int\limits_{m_j q_{j+1} m_{j+1}} k\frac{\partial\phi_h^*}{\partial\mathbf{n}} (\psi_h(q_{j+1}) - \psi_h) ds + \sum_{K\in\mathcal{T}_{h_p}} \sum_{j=1}^{3} \int\limits_{m_j q_{j+1} m_{j+1}} k\frac{\partial\phi_h^*}{\partial\mathbf{n}} \psi_h ds \\
&= \sum_{K\in\mathcal{T}_{h_p}} \sum_{j=1}^{3} \int\limits_{m_j q_{j+1} m_{j+1} \setminus \Gamma} k\frac{\partial\phi_h^*}{\partial\mathbf{n}} (\psi_h(q_{j+1}) - \psi_h) ds + \sum_{K\in\mathcal{T}_{h_p}} (k\nabla\phi_h^*, \nabla\psi_h)_K \\
&\quad + \sum_{K\in\mathcal{T}_{h_p}} \sum_{j=1}^{3} \int\limits_{m_j q_{j+1} m_{j+1} \bigcap \Gamma} k\frac{\partial\phi_h^*}{-\partial\mathbf{n}_f} (\psi_h(q_{j+1}) - \psi_h) ds + \sum_{K\in\mathcal{T}_{h_p}} (k\Delta\phi_h^*, \psi_h)_K \\
&= \sum_{K\in\mathcal{T}_{h_p}} \sum_{j=1}^{3} k\frac{\partial\phi_h^*}{\partial\mathbf{n}} \Big(\int\limits_{q_j m_j \bigcap \Omega_p \setminus \Gamma} \psi_h(q_j) ds + \int\limits_{m_j q_{j+1} \bigcap \Omega_p \setminus \Gamma} \psi_h(q_{j+1}) ds - \int\limits_{q_j q_{j+1} \bigcap \Omega_p \setminus \Gamma} \psi_h ds \Big) \\
&\quad + \sum_{n=1}^{N_p} \psi_h(p_n) \int\limits_{\partial K_n^* \bigcap \Omega_p \bigcap \Gamma} \mathbf{u}_h^* \cdot \mathbf{n}_f ds + \int\limits_{\Gamma} \mathbf{u}_h^* \cdot \mathbf{n}_f (-\psi_h) ds + \sum_{K\in\mathcal{T}_{h_p}} (k\nabla\phi_h^*, \nabla\psi_h)_K \\
&= \sum_{K\in\mathcal{T}_{h_p}} (k\nabla\phi_h^*, \nabla\psi_h)_K + \int\limits_{\Gamma} (\mathbf{u}_h^* \cdot \mathbf{n}_f)(\Gamma_{h_p}\psi_h - \psi_h) ds,
\end{aligned}$$

which completes the proof of Lemma 4.2.1. □

Lemma 4.2.2. *Let* $(\mathbf{u}_h^*, p_h^*, \phi_h^*) \in (\mathbf{X}_{h_f}, Q_{h_f}, X_{h_p})$ *be the solution of* (27). *For all* $(\mathbf{v}_h, q_h, \psi_h) \in (\mathbf{X}_{h_f}, Q_{h_f}, X_{h_p})$, *we have*

$$\tilde{a}_f(\mathbf{u}_h^*, \Gamma_{h_f}\mathbf{v}_h) = 2\nu \sum_{K\in\mathcal{T}_{h_f}} (\mathbb{D}(\mathbf{u}_h^*), \mathbb{D}(\mathbf{v}_h))_K + \int_\Gamma (p_h^* - g\phi_h^*)(\Gamma_{h_f}\mathbf{v}_h - \mathbf{v}_h)\cdot\mathbf{n}_f ds$$
$$- \frac{\alpha\nu\sqrt{d}}{\sqrt{trace(\mathbf{\Pi})}} \int_\Gamma \mathbf{P}_\tau(\mathbf{u}_h^*)\cdot\mathbf{P}_\tau(\Gamma_{h_f}\mathbf{v}_h - \mathbf{v}_h) ds.$$

Proof. $\forall\ \mathbf{u}_h^*, \mathbf{v}_h \in \mathbf{X}_{h_f}$, we can easily see that $\Delta\mathbf{u}_h^* = 0$, $\nabla(\mathbf{v}_h(q_{j+1})) = 0$ on each element and $\frac{\partial\mathbf{u}_h^*}{\partial\mathbf{n}}$ is a constant on $\partial K \setminus \Gamma$, $\forall\ K \in \mathcal{T}_{h_f}$. Similar to (34), we have [77]:

$$\int_{q_j m_j \bigcap \Omega_f\setminus\Gamma} \mathbf{v}_h(q_j) ds + \int_{m_j q_{j+1} \bigcap \Omega_f\setminus\Gamma} \mathbf{v}_h(q_{j+1}) ds = \int_{q_j q_{j+1} \bigcap \Omega_f\setminus\Gamma} \mathbf{v}_h ds. \tag{35}$$

By using Green's formula, (5)–(6), (16), and the above conclusions, we get

$$\begin{aligned}
&\tilde{a}_f(\mathbf{u}_h^*, \Gamma_{h_f}\mathbf{v}_h)\\
&= -\sum_{n=1}^{N_f} \mathbf{v}_h(p_n)\cdot \int_{\partial K_n^* \bigcap \Omega_f\setminus\Gamma} 2\nu\mathbb{D}(\mathbf{u}_h^*)\cdot\mathbf{n} ds\\
&= -\sum_{K\in\mathcal{T}_{h_f}}\sum_{j=1}^{3} \mathbf{v}_h(q_{j+1}) \int_{m_{j+1}cm_j} 2\nu\mathbb{D}(\mathbf{u}_h^*)\cdot\mathbf{n} ds\\
&= \sum_{K\in\mathcal{T}_{h_f}}\sum_{j=1}^{3} \int_{m_j q_{j+1} m_{j+1}} (2\nu\mathbb{D}(\mathbf{u}_h^*)\cdot\mathbf{n})\mathbf{v}_h(q_{j+1}) ds - \nu\sum_{K\in\mathcal{T}_{h_f}}\sum_{j=1}^{3} (\nabla\cdot(\mathbb{D}(\mathbf{u}_h^*)), \mathbf{v}_h(q_{j+1}))\mathfrak{R}_{j+1}\\
&\quad - \nu\sum_{K\in\mathcal{T}_{h_f}}\sum_{j=1}^{3} (\mathbb{D}(\mathbf{u}_h^*), \nabla(\mathbf{v}_h(q_{j+1})))\mathfrak{R}_{j+1}\\
&= \sum_{K\in\mathcal{T}_{h_f}}\sum_{j=1}^{3} \int_{m_j q_{j+1} m_{j+1}} 2\nu\mathbb{D}(\mathbf{u}_h^*)\cdot\mathbf{n}(\mathbf{v}_h(q_{j+1}) - \mathbf{v}_h) ds + \sum_{K\in\mathcal{T}_{h_f}}\sum_{j=1}^{3} \int_{m_j q_{j+1} m_{j+1}} 2\nu\mathbb{D}(\mathbf{u}_h^*)\cdot\mathbf{n}\mathbf{v}_h ds\\
&= \sum_{K\in\mathcal{T}_{h_f}}\sum_{j=1}^{3} \int_{m_j q_{j+1} m_{j+1}\setminus\Gamma} 2\nu\mathbb{D}(\mathbf{u}_h^*)\cdot\mathbf{n}(\mathbf{v}_h(q_{j+1}) - \mathbf{v}_h) ds + 2\nu\sum_{K\in\mathcal{T}_{h_f}} (\mathbb{D}(\mathbf{u}_h^*), \mathbb{D}(\mathbf{v}_h))_K\\
&\quad + \sum_{K\in\mathcal{T}_{h_f}}\sum_{j=1}^{3} \int_{m_j q_{j+1} m_{j+1} \bigcap \Gamma} 2\nu\mathbb{D}(\mathbf{u}_h^*)\cdot\mathbf{n}_f(\mathbf{v}_h(q_{j+1}) - \mathbf{v}_h) ds + 2\nu\sum_{K\in\mathcal{T}_{h_f}} (\mathbb{D}(\mathbf{u}_h^*), \mathbb{D}(\mathbf{v}_h))_K\\
&= \sum_{K\in\mathcal{T}_{h_f}}\sum_{j=1}^{3} \int_{m_j q_{j+1} m_{j+1}\setminus\Gamma} 2\nu\mathbb{D}(\mathbf{u}_h^*)\cdot\mathbf{n}(\mathbf{v}_h(q_{j+1}) - \mathbf{v}_h) ds + 2\nu\sum_{K\in\mathcal{T}_{h_f}} (\mathbb{D}(\mathbf{u}_h^*), \mathbb{D}(\mathbf{v}_h))_K\\
&\quad + \sum_{n=1}^{N_f} \mathbf{v}_h(p_n)\cdot \int_{\partial K_n^* \bigcap \Omega_f \bigcap \Gamma} 2\nu\mathbb{D}(\mathbf{u}_h^*)\cdot\mathbf{n}_f ds + \int_\Gamma \nu\frac{\partial\mathbf{u}_h^*}{\partial\mathbf{n}_f}\cdot(-\mathbf{v}_h) ds\\
&= \sum_{K\in\mathcal{T}_{h_f}}\sum_{j=1}^{3} 2\nu\mathbb{D}(\mathbf{u}_h^*)\cdot\mathbf{n}\Big(\int_{q_j m_j \bigcap \Omega_f\setminus\Gamma} \mathbf{v}_h(q_j) ds + \int_{m_j q_{j+1} \bigcap \Omega_f\setminus\Gamma} \mathbf{v}_h(q_{j+1}) ds - \int_{q_j q_{j+1} \bigcap \Omega_f\setminus\Gamma} \mathbf{v}_h ds\Big)\\
&\quad + \int_\Gamma ((2\nu\mathbb{D}(\mathbf{u}_h^*)\cdot\mathbf{n}_f\cdot\mathbf{n}_f)\cdot\mathbf{n}_f + (2\nu\mathbb{D}(\mathbf{u}_h^*)\cdot\mathbf{n}_f\cdot\tau)\cdot\tau)\cdot(\Gamma_{h_f}\mathbf{v}_h - \mathbf{v}_h) ds + 2\nu\sum_{K\in\mathcal{T}_{h_f}} (\mathbb{D}(\mathbf{u}_h^*), \mathbb{D}(\mathbf{v}_h))_K
\end{aligned}$$

$$
\begin{aligned}
&= \sum_{K\in\mathcal{T}_{h_f}}\sum_{j=1}^{3} 2\nu\mathbb{D}(\mathbf{u}_h^*)\cdot\mathbf{n}\Big(\int\limits_{q_jm_j\bigcap\Omega_f\backslash\Gamma}\mathbf{v}_h(q_j)ds+\int\limits_{m_jq_{j+1}\bigcap\Omega_f\backslash\Gamma}\mathbf{v}_h(q_{j+1})ds-\int\limits_{q_jq_{j+1}\bigcap\Omega_f\backslash\Gamma}\mathbf{v}_h ds\Big)\\
&\quad+\int\limits_{\Gamma}(p_h^*-g\phi_h^*)(\Gamma_{h_f}\mathbf{v}_h-\mathbf{v}_h)\cdot\mathbf{n}_f ds-\frac{\alpha\nu\sqrt{d}}{\sqrt{trace(\mathbf{\Pi})}}\int\limits_{\Gamma}\mathbf{P}_\tau(\mathbf{u}_h^*)\cdot\mathbf{P}_\tau(\Gamma_{h_f}\mathbf{v}_h-\mathbf{v}_h)ds\\
&\quad+2\nu\sum_{K\in\mathcal{T}_{h_f}}(\mathbb{D}(\mathbf{u}_h^*),\mathbb{D}(\mathbf{v}_h))_K\\
&=2\nu\sum_{K\in\mathcal{T}_{h_f}}(\mathbb{D}(\mathbf{u}_h^*),\mathbb{D}(\mathbf{v}_h))_K+\int\limits_{\Gamma}(p_h^*-g\phi_h^*)(\Gamma_{h_f}\mathbf{v}_h-\mathbf{v}_h)\cdot\mathbf{n}_f ds\\
&\quad-\frac{\alpha\nu\sqrt{d}}{\sqrt{trace(\mathbf{\Pi})}}\int\limits_{\Gamma}\mathbf{P}_\tau(\mathbf{u}_h^*)\cdot\mathbf{P}_\tau(\Gamma_{h_f}\mathbf{v}_h-\mathbf{v}_h)ds,
\end{aligned}
$$

which completes the proof of Lemma 4.2.2. □

Lemma 4.2.3. *Let* $(\mathbf{u}_h^*, p_h^*, \phi_h^*)\in(\mathbf{X}_{h_f}, Q_{h_f}^0, X_{h_p})$ *be the solution of* (27). *For all* $(\mathbf{v}_h, q_h, \psi_h)\in(\mathbf{X}_{h_f}, Q_{h_f}, X_{h_p})$, *we have*

$$\tilde{b}_f(\Gamma_{h_f}\mathbf{v}_h, p_h^*)=-(p_h^*,\nabla\cdot\mathbf{v}_h)+\int\limits_{\Gamma}((\mathbf{v}_h-\Gamma_{h_f}\mathbf{v}_h)\cdot\mathbf{n}_f)p_h^* ds.$$

Proof. $\forall\mathbf{v}_h\in\mathbf{X}_{h_f}$, $p_h^*\in Q_{h_f}^0$, we can easily get $\nabla p_h^*=0$, $\nabla\mathbf{v}_h(q_{j+1})=0$ on each element. By Green's formula, (35), and (16), we have

$$
\begin{aligned}
&\tilde{b}_f(\Gamma_{h_f}\mathbf{v}_h, p_h^*)\\
&=\sum_{n=1}^{N_f}\mathbf{v}_h(p_n)\cdot\int\limits_{\partial K_n^*\bigcap\Omega_f\backslash\Gamma}p_h^*\mathbf{n}ds\\
&=\sum_{K\in\mathcal{T}_{h_f}}\sum_{j=1}^{3}\int\limits_{m_{j+1}cm_j}p_h^*\mathbf{v}_h(q_{j+1})\cdot\mathbf{n}ds\\
&=-\sum_{K\in\mathcal{T}_{h_f}}\sum_{j=1}^{3}p_h^*\int\limits_{m_jq_{j+1}m_{j+1}}\mathbf{v}_h(q_{j+1})\cdot\mathbf{n}ds+\sum_{K\in\mathcal{T}_{h_f}}\sum_{j=1}^{3}(\nabla\cdot\mathbf{v}_h(q_{j+1}),p_h^*)_{\mathfrak{R}_{j+1}}\\
&\quad+\sum_{K\in\mathcal{T}_{h_f}}\sum_{j=1}^{3}(\mathbf{v}_h(q_{j+1}),\nabla p_h^*)_{\mathfrak{R}_{j+1}}\\
&=-\sum_{K\in\mathcal{T}_{h_f}}\sum_{j=1}^{3}p_h^*\int\limits_{m_jq_{j+1}m_{j+1}}(\mathbf{v}_h(q_{j+1})-\mathbf{v}_h)\cdot\mathbf{n}ds-\sum_{K\in\mathcal{T}_{h_f}}\sum_{j=1}^{3}p_h^*\int\limits_{m_jq_{j+1}m_{j+1}}\mathbf{v}_h\cdot\mathbf{n}ds\\
&=-\sum_{K\in\mathcal{T}_{h_f}}\sum_{j=1}^{3}p_h^*\int\limits_{m_jq_{j+1}m_{j+1}\backslash\Gamma}(\mathbf{v}_h(q_{j+1})-\mathbf{v}_h)\cdot\mathbf{n}ds-\sum_{K\in\mathcal{T}_{h_f}}\sum_{j=1}^{3}(\nabla\cdot\mathbf{v}_h,p_h^*)_{\mathfrak{R}_{j+1}}\\
&\quad+\sum_{K\in\mathcal{T}_{h_f}}\sum_{j=1}^{3}\int\limits_{m_jq_{j+1}m_{j+1}\bigcap\Gamma}(\mathbf{v}_h-\mathbf{v}_h(q_{j+1}))\cdot\mathbf{n}_f p_h^* ds-\sum_{K\in\mathcal{T}_{h_f}}\sum_{j=1}^{3}(\mathbf{v}_h,\nabla p_h^*)_{\mathfrak{R}_{j+1}}\\
&=-\sum_{K\in\mathcal{T}_{h_f}}\sum_{j=1}^{3}p_h^*\Big(\int\limits_{q_jm_j\bigcap\Omega_f\backslash\Gamma}\mathbf{v}_h(q_j)ds+\int\limits_{m_jq_{j+1}\bigcap\Omega_f\backslash\Gamma}\mathbf{v}_h(q_{j+1})ds-\int\limits_{q_jq_{j+1}\bigcap\Omega_f\backslash\Gamma}\mathbf{v}_h ds\Big)
\end{aligned}
$$

$$
\begin{aligned}
&-(p_h^*, \nabla\cdot\mathbf{v}_h) - \sum_{n=1}^{N_f}\mathbf{v}_h(p_n)\cdot \int\limits_{\partial K_n^* \bigcap \Omega_f \bigcap \Gamma} p_h^*\mathbf{n}_f ds + \int\limits_{\Gamma}(\mathbf{v}_h\cdot\mathbf{n}_f)p_h^* ds\\
&= -(p_h^*, \nabla\cdot\mathbf{v}_h) + \int\limits_{\Gamma}((\mathbf{v}_h - \Gamma_{h_f}\mathbf{v}_h)\cdot\mathbf{n}_f)p_h^* ds,
\end{aligned}
$$

which completes the proof of Lemma 4.2.3. □

Lemma 4.2.4. *Let* $(\mathbf{u}_h^*, p_h^*, \phi_h^*) \in (\mathbf{X}_{h_f}, Q_{h_f}^1, X_{h_p})$ *be the solution of* (27). *For all* $(\mathbf{v}_h, q_h, \psi_h) \in (\mathbf{X}_{h_f}, Q_{h_f}, X_{h_p})$, *we have*

$$
\tilde{b}_f(\Gamma_{h_f}\mathbf{v}_h, p_h^*) = -(p_h^*, \nabla\cdot\mathbf{v}_h) + \int\limits_{\Gamma}((\mathbf{v}_h - \Gamma_{h_f}\mathbf{v}_h)\cdot\mathbf{n}_f)p_h^* ds.
$$

Proof. $\forall\mathbf{v}_h \in \mathbf{X}_{h_f}$, $p_h^* \in Q_{h_f}^1$, we can easily get ∇p_h^* is a constant on each element, by Green's formula, together with (18), we have

$$
\begin{aligned}
&\tilde{b}_f(\Gamma_{h_f}\mathbf{v}_h, p_h^*)\\
&= \sum_{n=1}^{N_f}\mathbf{v}_h(p_n)\cdot \int\limits_{\partial K_n^* \bigcap \Omega_f\setminus\Gamma} p_h^*\mathbf{n} ds\\
&= \sum_{n=1}^{N_f}\mathbf{v}_h(p_n)\cdot \int\limits_{\partial K_n^* \bigcap \Omega_f} p_h^*\mathbf{n} ds - \sum_{n=1}^{N_f}\mathbf{v}_h(p_n)\cdot \int\limits_{\partial K_n^* \bigcap \Omega_f \bigcap \Gamma} p_h^*\mathbf{n} ds\\
&= \sum_{n=1}^{N_f}\int\limits_{K_n^* \bigcap \Omega_f} \nabla\cdot\mathbf{v}_h(p_n)p_h^* dx + \sum_{n=1}^{N_f}\int\limits_{K_n^* \bigcap \Omega_f}\mathbf{v}_h(p_n)\cdot\nabla p_h^* dx - \int\limits_{\Gamma}(\Gamma_{h_f}\mathbf{v}_h\cdot\mathbf{n}_f)p_h^* ds\\
&= \sum_{K\in\mathcal{T}_{h_f}}\int\limits_{K}\Gamma_{h_f}\mathbf{v}_h\cdot\nabla p_h^* dx - \int\limits_{\Gamma}(\Gamma_{h_f}\mathbf{v}_h\cdot\mathbf{n}_f)p_h^* ds\\
&= \sum_{K\in\mathcal{T}_{h_f}}\int\limits_{K}(\Gamma_{h_f}\mathbf{v}_h - \mathbf{v}_h)\cdot\nabla p_h^* dx + \sum_{K\in\mathcal{T}_{h_f}}\int\limits_{K}\mathbf{v}_h\cdot\nabla p_h^* dx - \int\limits_{\Gamma}(\Gamma_{h_f}\mathbf{v}_h\cdot\mathbf{n}_f)p_h^* ds\\
&= -(p_h^*, \nabla\cdot\mathbf{v}_h) + \int\limits_{\Gamma}((\mathbf{v}_h - \Gamma_{h_f}\mathbf{v}_h)\cdot\mathbf{n}_f)p_h^* ds,
\end{aligned}
$$

which completes the proof of Lemma 4.2.4. □

Combining the above four lemmas, we obtain the following equivalence relationship between the stabilized finite volume element and stabilized finite element approximations for the coupled steady Stokes–Darcy problem:

Theorem 4.2.1. *Let* $(\mathbf{u}_h^*, p_h^*, \phi_h^*) \in (\mathbf{X}_{h_f}, Q_{h_f}, X_{h_p})$ *be the solution of* (27). *For all* $(\mathbf{v}_h, q_h, \psi_h) \in (\mathbf{X}_{h_f}, Q_{h_f}, X_{h_p})$, *we have*

$$
\tilde{B}_h^*((\mathbf{u}_h^*, p_h^*, \phi_h^*), (\mathbf{v}_h, q_h, \psi_h)) = \tilde{B}_h((\mathbf{u}_h^*, p_h^*, \phi_h^*), (\mathbf{v}_h, q_h, \psi_h)). \tag{36}
$$

Proof. By using the definition of $\tilde{B}_h^*((\cdot,\cdot,\cdot),(\cdot,\cdot,\cdot))$ in (26) and the above four lemmas, we have

$$
\begin{aligned}
&\tilde{B}_h^*((\mathbf{u}_h^*, p_h^*, \phi_h^*), (\mathbf{v}_h, q_h, \psi_h))\\
&= \tilde{a}_f(\mathbf{u}_h^*, \Gamma_{h_f}\mathbf{v}_h) + \tilde{b}_f(\Gamma_{h_f}\mathbf{v}_h, p_h^*) + g\tilde{a}_p(\phi_h^*, \Gamma_{h_p}\psi_h) + \langle g\phi_h^*, \Gamma_{h_f}\mathbf{v}_h\cdot\mathbf{n}_f\rangle_\Gamma\\
&\quad - g\langle\mathbf{u}_h^*\cdot\mathbf{n}_f, \Gamma_{h_p}\psi_h\rangle_\Gamma + \frac{\alpha\nu\sqrt{d}}{\sqrt{trace(\mathbf{\Pi})}}\langle\mathbf{P}_\tau(\mathbf{u}_h^*), \mathbf{P}_\tau(\Gamma_{h_f}\mathbf{v}_h)\rangle_\Gamma + b_f(\mathbf{u}_h^*, q_h) + G(p_h^*, q_h)\\
&= 2\nu\sum_{K\in\mathcal{T}_{h_f}}(\mathbb{D}(\mathbf{u}_h^*), \mathbb{D}(\mathbf{v}_h))_K + \int\limits_{\Gamma}(p_h^* - g\phi_h^*)(\Gamma_{h_f}\mathbf{v}_h - \mathbf{v}_h)\cdot\mathbf{n}_f ds
\end{aligned}
$$

$$
\begin{aligned}
&- \frac{\alpha\nu\sqrt{d}}{\sqrt{trace(\mathbf{\Pi})}} \int_\Gamma \mathbf{P}_\tau(\mathbf{u}_h^*)\cdot\mathbf{P}_\tau(\Gamma_{h_f}\mathbf{v}_h - \mathbf{v}_h)ds - (p_h^*, \nabla\cdot\mathbf{v}_h) + b_f(\mathbf{u}_h^*, q_h) + G(p_h^*, q_h)\\
&+ \int_\Gamma ((\mathbf{v}_h - \Gamma_{h_f}\mathbf{v}_h)\cdot\mathbf{n}_f)p_h^* ds + \sum_{K\in\mathcal{T}_{h_p}} gk(\nabla\phi_h^*, \nabla\psi_h)_K + \int_\Gamma g\mathbf{u}_h^*\cdot\mathbf{n}_f(\Gamma_{h_p}\psi_h - \psi_h)ds\\
&+ \langle g\phi_h^*, \Gamma_{h_f}\mathbf{v}_h\cdot\mathbf{n}_f\rangle_\Gamma - g\langle\mathbf{u}_h^*\cdot\mathbf{n}_f, \Gamma_{h_p}\psi_h\rangle_\Gamma + \frac{\alpha\nu\sqrt{d}}{\sqrt{trace(\mathbf{\Pi})}}\langle\mathbf{P}_\tau(\mathbf{u}_h^*), \mathbf{P}_\tau(\Gamma_{h_f}\mathbf{v}_h)\rangle_\Gamma.
\end{aligned}
$$

Re-organizing the terms in the above equation and using the definition of $\tilde{B}_h((\cdot,\cdot,\cdot),(\cdot,\cdot,\cdot))$ in (29), we get

$$
\begin{aligned}
&\tilde{B}_h^*((\mathbf{u}_h^*, p_h^*, \phi_h^*), (\mathbf{v}_h, q_h, \psi_h))\\
&= 2\nu\sum_{K\in\mathcal{T}_{h_f}} (\mathbb{D}(\mathbf{u}_h^*), \mathbb{D}(\mathbf{v}_h))_K + \int_\Gamma g\phi_h^*\mathbf{v}_h\cdot\mathbf{n}_f ds + \frac{\alpha\nu\sqrt{d}}{\sqrt{trace(\mathbf{\Pi})}}\int_\Gamma \mathbf{P}_\tau\mathbf{u}_h^*\cdot\mathbf{P}_\tau\mathbf{v}_h ds\\
&\quad - (p_h^*, \nabla\cdot\mathbf{v}_h) + \sum_{K\in\mathcal{T}_{h_p}} gk(\nabla\phi_h^*, \nabla\psi_h)_K - \int_\Gamma g\mathbf{u}_h^*\cdot\mathbf{n}_f\psi_h ds + b_f(\mathbf{u}_h^*, q_h) + G(p_h^*, q_h)\\
&\quad + \left[\int_\Gamma p_h^*(\Gamma_{h_f}\mathbf{v}_h - \mathbf{v}_h)\cdot\mathbf{n}_f ds + \int_\Gamma ((\mathbf{v}_h - \Gamma_{h_f}\mathbf{v}_h)\cdot\mathbf{n}_f)p_h^* ds\right]\\
&\quad + \left[\frac{\alpha\nu\sqrt{d}}{\sqrt{trace(\mathbf{\Pi})}}\langle\mathbf{P}_\tau(\mathbf{u}_h^*), \mathbf{P}_\tau(\Gamma_{h_f}\mathbf{v}_h)\rangle_\Gamma - \frac{\alpha\nu\sqrt{d}}{\sqrt{trace(\mathbf{\Pi})}}\int_\Gamma \mathbf{P}_\tau(\mathbf{u}_h^*)\cdot\mathbf{P}_\tau(\Gamma_{h_f}\mathbf{v}_h)ds\right]\\
&\quad + \left[\langle g\phi_h^*, \Gamma_{h_f}\mathbf{v}_h\cdot\mathbf{n}_f\rangle_\Gamma + \int_\Gamma (-g\phi_h^*)(\Gamma_{h_f}\mathbf{v}_h)\cdot\mathbf{n}_f ds\right] + \left[\int_\Gamma g\mathbf{u}_h^*\cdot\mathbf{n}_f\Gamma_{h_p}\psi_h ds - g\langle\mathbf{u}_h^*\cdot\mathbf{n}_f, \Gamma_{h_p}\psi_h\rangle_\Gamma\right]\\
&= 2\nu\sum_{K\in\mathcal{T}_{h_f}} (\mathbb{D}(\mathbf{u}_h^*), \mathbb{D}(\mathbf{v}_h))_K + \int_\Gamma g\phi_h^*\mathbf{v}_h\cdot\mathbf{n}_f ds + \frac{\alpha\nu\sqrt{d}}{\sqrt{trace(\mathbf{\Pi})}}\int_\Gamma \mathbf{P}_\tau\mathbf{u}_h^*\cdot\mathbf{P}_\tau\mathbf{v}_h ds\\
&\quad - (p_h^*, \nabla\cdot\mathbf{v}_h) + \sum_{K\in\mathcal{T}_{h_p}} gk(\nabla\phi_h^*, \nabla\psi_h)_K - \int_\Gamma g\mathbf{u}_h^*\cdot\mathbf{n}_f\psi_h ds + b_f(\mathbf{u}_h^*, q_h) + G(p_h^*, q_h)\\
&= \tilde{B}_h((\mathbf{u}_h^*, p_h^*, \phi_h^*), (\mathbf{v}_h, q_h, \psi_h)),
\end{aligned}
$$

which completes the proof of Theorem 4.2.1. □

Remark 4.2.1. In Theorem 4.2.1, we prove the equivalence relationship for the Stokes–Darcy model with the Beavers–Joseph–Saffman–Jones interface condition. If one uses the Beavers–Joseph interface condition [4] instead of the Beavers–Joseph–Saffman–Jones interface condition, the proof will be similar with the same steps. The major difficulty of adopting the Beavers–Joseph interface condition arises from the coercivity of the bilinear form. But this difficulty was already addressed in [13–15,34]. Specifically, in the proof we only need to replace the interface term $\mathbf{P}_\tau(\mathbf{u}_h^*)$ by $\mathbf{P}_\tau(\mathbf{u}_h^* + \mathbb{K}\nabla\phi_h^*)$ for Beavers–Joseph interface condition and then apply the well-posedness theory in [14] to deal with this additional term.

Remark 4.2.2. Most existing finite volume methods of Stokes equations are restricted to the cases where the velocity and pressure fields are approximated by piecewise linear or piecewise constants polynomials [27,57,77,78]. The linear finite volume scheme can be considered as a small perturbation of its corresponding finite element scheme, and the corresponding difference term was well estimated in the literature. This leads to the equivalence between the linear finite volume scheme and the linear finite element scheme. However, this is not the case for the high order finite volume schemes. Hence the estimate of the difference term is a challenging task. In fact, the necessary and sufficient conditions for the uniform ellipticity of the bilinear forms of the higher-order finite volume schemes need to be established in terms of geometric requirements on triangle meshes [76]. Another main difficulty in the analysis for higher-order finite volume schemes of Stokes equation is to verify the inf-sup conditions for the discrete systems. Hence it is an interesting future work to study the higher-order finite volume schemes for the Stokes–Darcy model.

4.3. Convergence analysis

In this subsection, we show the optimal error estimates for the velocity, pressure, and hydraulic head. Note that from the equivalence relationship between the stabilized finite volume element and stabilized finite element approximations in the Theorem 4.2.1, we can obtain the following results about the bilinear form $\tilde{B}_h^*((\cdot,\cdot,\cdot),(\cdot,\cdot,\cdot))$.

Theorem 4.3.1. *The bilinear form $\tilde{B}_h^*((\mathbf{u}_h^*, p_h^*, \phi_h^*), (\mathbf{v}_h, q_h, \psi_h))$ satisfies the continuity property*

$$\tilde{B}_h^*((\mathbf{u}_h^*, p_h^*, \phi_h^*), (\mathbf{v}_h, q_h, \psi_h)) \le C(\|\mathbf{u}_h^*\|_1 + \|\phi_h^*\|_1 + \|p_h^*\|_0)(\|\mathbf{v}_h\|_1 + \|\psi_h\|_1 + \|q_h\|_0), \tag{37}$$

and the coercive property

$$\sup_{0\neq(\mathbf{v}_h,q_h,\psi_h)\in(\mathbf{X}_{h_f},Q_{h_f},X_{h_p})} \frac{|\tilde{B}_h^*((\mathbf{u}_h^*, p_h^*, \phi_h^*), (\mathbf{v}_h, q_h, \psi_h))|}{(\|\mathbf{v}_h\|_1^2 + \|q_h\|_0^2 + \|\psi_h\|_1^2)^{\frac{1}{2}}} \ge \beta(\|\mathbf{u}_h^*\|_1^2 + \|p_h^*\|_0^2 + \|\phi_h^*\|_1^2)^{\frac{1}{2}}, \tag{38}$$

for all $(\mathbf{u}_h^*, p_h^*, \phi_h^*)$, $(\mathbf{v}_h, q_h, \psi_h) \in (\mathbf{X}_{h_f}, Q_{h_f}, X_{h_p})$, where β is a positive constant depending only on domain.

Now we will show the main convergence analysis result as follows.

Theorem 4.3.2. *Let $(\mathbf{u}, p, \phi)$ and $(\mathbf{u}_h^*, p_h^*, \phi_h^*)$ be the solutions of (9) and (27), respectively. Then we have*

$$\|\mathbf{u} - \mathbf{u}_h^*\|_1 + \|p - p_h^*\|_0 + \|\phi - \phi_h^*\|_1 \le Ch(\|\mathbf{u}\|_2 + \|p\|_1 + \|\phi\|_2 + \|\mathbf{f}_f\|_0 + \|f_p\|_0), \tag{39}$$

and

$$\|\mathbf{u} - \mathbf{u}_h^*\|_0 + \|\phi - \phi_h^*\|_0 \le Ch^2(\|\mathbf{u}\|_2 + \|p\|_1 + \|\phi\|_2 + \|\mathbf{f}_f\|_1 + \|f_p\|_1). \tag{40}$$

Proof. Choose $(\mathbf{v}, q, \psi) = (\mathbf{v}_h, q_h, \psi_h)$ in (9). By subtracting (27) from (9) and using (36), we have

$$\tilde{B}_h((\mathbf{u} - \mathbf{u}_h^*, p - p_h^*, \phi - \phi_h^*), (\mathbf{v}_h, q_h, \psi_h)) - G(p, q_h) = (\mathbf{f}_f, \mathbf{v}_h - \Gamma_{h_f}\mathbf{v}_h) + g(f_p, \psi_h - \Gamma_{h_p}\psi_h). \tag{41}$$

Using Cauchy–Schwarz inequality and (19), we have

$$|(\mathbf{f}_f, \mathbf{v}_h - \Gamma_{h_f}\mathbf{v}_h) + g(f_p, \psi_h - \Gamma_{h_p}\psi_h)| \le Ch(\|\mathbf{f}_f\|_0\|\mathbf{v}_h\|_1 + \|f_p\|_0\|\psi_h\|_1). \tag{42}$$

Setting $(\mathbf{e}, \eta, \xi) = (I_h\mathbf{u} - \mathbf{u}_h^*, \rho_h p - p_h^*, J_h\phi - \phi_h^*)$ and using Cauchy–Schwarz inequality, (21), (30), (42), (23)–(24), and (10)–(12), we deduce that

$$\begin{aligned}
&\tilde{B}_h((\mathbf{e}, \eta, \xi), (\mathbf{v}_h, q_h, \psi_h)) \\
&= G(p, q_h) + (\mathbf{f}_f, \mathbf{v}_h - \Gamma_{h_f}\mathbf{v}_h) + g(f_p, \psi_h - \Gamma_{h_p}\psi_h) \\
&\quad - \tilde{B}_h((\mathbf{u} - I_h\mathbf{u}, p - \rho_h p, \phi - J_h\phi), (\mathbf{v}_h, q_h, \psi_h)) \\
&\le |G(p, q_h)| + |(\mathbf{f}_f, \mathbf{v}_h - \Gamma_{h_f}\mathbf{v}_h) + g(f_p, \psi_h - \Gamma_{h_p}\psi_h)| \\
&\quad + |\tilde{B}_h((\mathbf{u} - I_h\mathbf{u}, p - \rho_h p, \phi - J_h\phi), (\mathbf{v}_h, q_h, \psi_h))| \\
&\le C\|p - \Pi_h p\|_0(\|q_h\|_0 + \|\Pi_h q_h\|_0) + Ch(\|\mathbf{f}_f\|_0\|\mathbf{v}_h\|_1 + \|f_p\|_0\|\psi_h\|_1) \\
&\quad + C(\|\mathbf{u} - I_h\mathbf{u}\|_1 + \|p - \rho_h p\|_0 + \|\phi - J_h\phi\|_1)(\|\mathbf{v}_h\|_1 + \|q_h\|_0 + \|\psi_h\|_1) \\
&\le Ch\|p\|_1\|q_h\|_0 + Ch(\|\mathbf{f}_f\|_0\|\mathbf{v}_h\|_1 + \|f_p\|_0\|\psi_h\|_1) \\
&\quad + Ch(\|\mathbf{u}\|_2 + \|p\|_1 + \|\phi\|_2)(\|\mathbf{v}_h\|_1 + \|q_h\|_0 + \|\psi_h\|_1) \\
&\le Ch(\|\mathbf{u}\|_2 + \|p\|_1 + \|\phi\|_2 + \|\mathbf{f}_f\|_0 + \|f_p\|_0)(\|\mathbf{v}_h\|_1 + \|q_h\|_0 + \|\psi_h\|_1).
\end{aligned} \tag{43}$$

Using (31) and (43), we deduce that

$$\begin{aligned}
\beta(\|\mathbf{e}\|_1^2 + \|\eta\|_0^2 + \|\xi\|_1^2)^{\frac{1}{2}} &\le \sup_{0\neq(\mathbf{v}_h,q_h,\psi_h)\in(\mathbf{X}_{h_f},Q_{h_f},X_{h_p})} \frac{|\tilde{B}_h((\mathbf{e}, \eta, \xi), (\mathbf{v}_h, q_h, \psi_h))|}{(\|\mathbf{v}_h\|_1^2 + \|q_h\|_0^2 + \|\psi_h\|_1^2)^{\frac{1}{2}}} \\
&\le Ch(\|\mathbf{u}\|_2 + \|p\|_1 + \|\phi\|_2 + \|\mathbf{f}_f\|_0 + \|f_p\|_0).
\end{aligned} \tag{44}$$

Using the triangle inequality and (10)–(12), we have

$$
\begin{aligned}
&\|\mathbf{u}-\mathbf{u}_h^*\|_1+\|p-p_h^*\|_0+\|\phi-\phi_h^*\|_1\\
&=\|\mathbf{u}-I_h\mathbf{u}+I_h\mathbf{u}-\mathbf{u}_h^*\|_1+\|p-\rho_h p+\rho_h p-p_h^*\|_0+\|\phi-J_h\phi+J_h\phi-\phi_h^*\|_1\\
&\le\|\mathbf{u}-I_h\mathbf{u}\|_1+\|p-\rho_h p\|_0+\|\phi-J_h\phi\|_1+\|\mathbf{e}\|_1+\|\eta\|_0+\|\xi\|_1\\
&\le Ch(\|\mathbf{u}\|_2+\|p\|_1+\|\phi\|_2+\|\mathbf{f}_f\|_0+\|f_p\|_0).
\end{aligned}
$$

Thus, we obtain (39). □

The L^2-error estimate is obtained using the Aubin–Nitsche duality argument. Let $(\mathbf{u}, p, \phi)$ and $(\mathbf{u}_h^*, p_h^*, \phi_h^*)$ be the solutions of (9) and (27), respectively. The dual problem is to find $(\mathbf{w}, r, \xi) \in \mathbf{X}_f \times Q_f \times X_p$ such that, $\forall(\mathbf{v}, q, \psi) \in \mathbf{X}_f \times Q_f \times X_p$,

$$
B((\mathbf{v},q,\psi),(\mathbf{w},r,\xi))=\int_{\Omega_f}(\mathbf{u}-\mathbf{u}_h^*)\mathbf{v}+\int_{\Omega_p}(\phi-\phi_h^*)\psi. \tag{45}
$$

The solution of the dual problem (45) has the regularity:

$$
\|\mathbf{w}\|_2+\|r\|_1+\|\xi\|_2\le C(\|\phi-\phi_h^*\|_0+\|\mathbf{u}-\mathbf{u}_h^*\|_0). \tag{46}
$$

Subtracting (27) with $(\mathbf{v}_h,\, q_h,\, \psi_h) = (I_h\mathbf{w},\, \rho_h r,\, J_h\xi)$ from (9) with $(\mathbf{v},\, q,\, \psi) = (I_h\mathbf{w},\, \rho_h r,\, J_h\xi)$ and using (36), we have

$$
\begin{aligned}
&\tilde{B}_h((\mathbf{u}-\mathbf{u}_h^*,p-p_h^*,\phi-\phi_h^*),(I_h\mathbf{w},\rho_h r,J_h\xi))\\
&=G(p,\rho_h r)+(\mathbf{f}_f,I_h\mathbf{w}-\Gamma_{h_f}I_h\mathbf{w})+g(f_p,J_h\xi-\Gamma_{h_p}J_h\xi).
\end{aligned} \tag{47}
$$

Choosing $(\mathbf{v}, q, \psi) = (\mathbf{u}-\mathbf{u}_h^*, p-p_h^*, \phi-\phi_h^*)$ in (45) and using (47), we obtain

$$
\begin{aligned}
&\|\mathbf{u}-\mathbf{u}_h^*\|_0^2+\|\phi-\phi_h^*\|_0^2\\
&=B((\mathbf{u}-\mathbf{u}_h^*,p-p_h^*,\phi-\phi_h^*),(\mathbf{w},r,\xi))\\
&=\tilde{B}_h((\mathbf{u}-\mathbf{u}_h^*,p-p_h^*,\phi-\phi_h^*),(\mathbf{w},r,\xi))-G(p-p_h^*,r)\\
&=\tilde{B}_h((\mathbf{u}-\mathbf{u}_h^*,p-p_h^*,\phi-\phi_h^*),(\mathbf{w}-I_h\mathbf{w},r-\rho_h r,\xi-J_h\xi))\\
&\quad+\tilde{B}_h((\mathbf{u}-\mathbf{u}_h^*,p-p_h^*,\phi-\phi_h^*),(I_h\mathbf{w},\rho_h r,J_h\xi))-G(p-p_h^*,r)\\
&=\tilde{B}_h((\mathbf{u}-\mathbf{u}_h^*,p-p_h^*,\phi-\phi_h^*),(\mathbf{w}-I_h\mathbf{w},r-\rho_h r,\xi-J_h\xi))\\
&\quad+G(p,\rho_h r)+(\mathbf{f}_f,I_h\mathbf{w}-\Gamma_{h_f}I_h\mathbf{w})+g(f_p,J_h\xi-\Gamma_{h_p}J_h\xi)-G(p-p_h^*,r).
\end{aligned} \tag{48}
$$

Using (30), (39), (10)–(12) and (46), we have

$$
\begin{aligned}
&|\tilde{B}_h((\mathbf{u}-\mathbf{u}_h^*,p-p_h^*,\phi-\phi_h^*),(\mathbf{w}-I_h\mathbf{w},r-\rho_h r,\xi-J_h\xi))|\\
&\le C(\|\mathbf{u}-\mathbf{u}_h^*\|_1+\|p-p_h^*\|_0+\|\phi-\phi_h^*\|_1)(\|\mathbf{w}-I_h\mathbf{w}\|_1+\|r-\rho_h r\|_0+\|\xi-J_h\xi\|_1)\\
&\le Ch^2(\|\mathbf{u}\|_2+\|p\|_1+\|\phi\|_2+\|\mathbf{f}_f\|_0+\|f_p\|_0)(\|\mathbf{w}\|_2+\|r\|_1+\|\xi\|_2)\\
&\le Ch^2(\|\mathbf{u}\|_2+\|p\|_1+\|\phi\|_2+\|\mathbf{f}_f\|_0+\|f_p\|_0)(\|\mathbf{u}-\mathbf{u}_h^*\|_0+\|\phi-\phi_h^*\|_0).
\end{aligned} \tag{49}
$$

Using (21), Cauchy–Schwarz inequality and (24), (12), (46), we have

$$
\begin{aligned}
&|G(p,\rho_h r)|\\
&=|G(p,\rho_h r-r)+G(p,r)|\\
&\le C\|p-\Pi_h p\|_0\|\rho_h r-r\|_0+C\|p-\Pi_h p\|_0\|\Pi_h(\rho_h r-r)\|_0+C\|p-\Pi_h p\|_0\|r-\Pi_h r\|_0\\
&\le C\|p-\Pi_h p\|_0\|\rho_h r-r\|_0+C\|p-\Pi_h p\|_0\|r-\Pi_h r\|_0\\
&\le Ch^2\|p\|_1\|r\|_1\\
&\le Ch^2\|p\|_1(\|\mathbf{u}-\mathbf{u}_h^*\|_0+\|\phi-\phi_h^*\|_0).
\end{aligned} \tag{50}
$$

Using (21), Cauchy–Schwarz inequality and (23)–(24), (39), (46), we have

$$
\begin{aligned}
&|G(p-p_h^*, r)| \\
&\le C\|p-p_h^*\|_0\|r-\Pi_h r\|_0 + C\|\Pi_h(p-p_h^*)\|_0\|r-\Pi_h r\|_0 \\
&\le C\|p-p_h^*\|_0\|r-\Pi_h r\|_0 \\
&\le Ch\|p-p_h^*\|_0\|r\|_1 \\
&\le Ch^2(\|\mathbf{u}\|_2+\|p\|_1+\|\phi\|_2+\|\mathbf{f}_f\|_0+\|f_p\|_0)(\|\mathbf{u}-\mathbf{u}_h^*\|_0+\|\phi-\phi_h^*\|_0).
\end{aligned} \tag{51}
$$

Using (18)–(19), Cauchy–Schwarz inequality, (22), (24), (13)–(14), and (46), we have

$$
\begin{aligned}
&|(\mathbf{f}_f, I_h\mathbf{w}-\Gamma_{h_f}I_h\mathbf{w}) + g(f_p, J_h\xi-\Gamma_{h_p}J_h\xi)| \\
&= |(\mathbf{f}_f-\Pi_h^0\mathbf{f}_f, I_h\mathbf{w}-\Gamma_{h_f}I_h\mathbf{w}) + g(f_p-\Pi_h^0 f_p, J_h\xi-\Gamma_{h_p}J_h\xi)| \\
&\le C(\|\mathbf{f}_f-\Pi_h^0\mathbf{f}_f\|_0\|I_h\mathbf{w}-\Gamma_{h_f}I_h\mathbf{w}\|_0 + \|f_p-\Pi_h^0 f_p\|_0\|J_h\xi-\Gamma_{h_p}J_h\xi\|_0 \\
&\le Ch^2(\|\mathbf{f}_f\|_1\|I_h\mathbf{w}\|_1 + \|f_p\|_1\|J_h\xi\|_1) \\
&\le Ch^2(\|\mathbf{f}_f\|_1\|\mathbf{w}\|_2 + \|f_p\|_1\|\xi\|_2) \\
&\le Ch^2(\|\mathbf{f}_f\|_1+\|f_p\|_1)(\|\mathbf{u}-\mathbf{u}_h^*\|_0+\|\phi-\phi_h^*\|_0).
\end{aligned} \tag{52}
$$

Plugging (49)–(52) into (48), we obtain (40). □

5. Numerical experiments

In this section, we will give four numerical experiments to illustrate the features of the presented method for the coupled Stokes–Darcy system, including the optimal accuracy orders, mass conservation, capability to conveniently deal with complicated geometries, and applicability to realistic parameters and problems.

An implicit treatment of the projection operator Π_h was used in [6] for the implementation of the stabilized term. In this paper we consider another implementation technique, which provides an explicit computation for Π_h or $I-\Pi_h$ at the element level with the standard nodal data structures. In the following we will briefly discuss about the explicit computation for Π_h^0 based on two local quadrature rules [57] and Π_h^1 based on Clement-like interpolation [79].

A suitable choice of $I-\Pi_h^0$ based on two local Gaussian quadrature rules is given by [57]:

$$
\|(I-\Pi_h^0)p_h\|_0 = \left\{ \int_{K,j(j\ge 2)} (p_h)^2 \mathrm{d}x - \int_{K,1} (p_h)^2 \mathrm{d}x \right\}^{1/2}, \quad \forall p_h \in Q_{h_f}^1,\ K \in \mathcal{T}_{h_f}. \tag{53}
$$

Here

$$
\int_{K,k} g(x)\mathrm{d}x = \sum_{I=1}^{N(k)} g(x_I) w_I,
$$

where x_I is the quadrature point, w_I is the quadrature weight, and $N(k)$ represents the total number of quadrature points. Hence it is easy to see that $I-\Pi_h^0$ can be explicitly computed at the element level to obtain the results equivalent to that of the implicit treatment. And the stabilization term can be computed by

$$
G(p_h, q_h) = \sum_{K\in\mathcal{T}_{h_f}} \left\{ \int_{K,j(j\ge 2)} (p_h * q_h)dx - \int_{K,1} (p_h * q_h)dx \right\}, \quad \forall K \in \mathcal{T}_{h_f}, \forall p_h,\ q_h \in Q_{h_f}^1. \tag{54}
$$

A suitable choice of Π_h^1 is to define its interpolation by using a projection onto the dual volume associated with each node [79]. For each node $p_j \in \mathcal{N}_f$, $j=1, 2, \cdots, N_f$, let $S_j \subset \Omega_f$ denote the union of triangles that share the common vertex p_j, and ϕ_j denote the continuous, piecewise linear basis function such that $\phi_j(p_m)=\delta_{j,m}$. We define $I-\Pi_h^1$ based on Clement-like interpolation:

$$
\|(I-\Pi_h^1)p_h\|_{0,K} = \|p_h - \sum_{p_j\in K} w_j\phi_j\|_{0,K}, \quad \forall K \in \mathcal{T}_{h_f}, j=1, 2, \cdots, N_f. \tag{55}
$$

w_j can be computed by following formula:

$$
w_j = \frac{\sum_{K\in S_j} V_j(K) p_K}{\sum_{K\in S_j} V_j(K)}, \tag{56}
$$

Table 1
Errors of the P_1–P_0–P_1 with explicit implementation of the stabilization term.

$\frac{1}{h}$	$\|\mathbf{u}_f - \mathbf{u}_f{}^h\|_0$	$\|\mathbf{u}_f - \mathbf{u}_f{}^h\|_1$	$\|p - p_h\|_0$	$\|\phi_p - \phi_p{}^h\|_0$	$\|\phi_p - \phi_p{}^h\|_1$
4	3.9148E−2	5.4441E−1	1.4616E−1	1.4548E−2	2.9927E−1
8	1.0092E−2	2.8015E−1	6.9687E−2	3.6620E−3	1.4983E−1
16	2.5360E−3	1.4105E−1	2.8983E−2	9.1678E−4	7.4942E−2
32	6.3399E−4	7.0641E−2	1.2923E−2	2.2919E−4	3.7474E−2
64	1.5846E−4	3.5333E−2	6.1567E−3	5.7285E−5	1.8738E−2
Rate	1.9872	0.9864	1.1414	1.9971	0.9994

Table 2
Errors of the P_1–P_0–P_1 with implicit implementation of the stabilization term.

$\frac{1}{h}$	$\|\mathbf{u}_f - \mathbf{u}_f{}^h\|_0$	$\|\mathbf{u}_f - \mathbf{u}_f{}^h\|_1$	$\|p - p_h\|_0$	$\|\phi_p - \phi_p{}^h\|_0$	$\|\phi_p - \phi_p{}^h\|_1$
4	3.9342E−2	5.4427E−1	1.8499E−1	1.4549E−2	2.9927E−1
8	1.0117E−2	2.8017E−1	7.9226E−2	3.6614E−3	1.4983E−1
16	2.5364E−3	1.4106E−1	3.0841E−2	9.1657E−4	7.4942E−2
32	6.3389E−4	7.0642E−2	1.3278E−2	2.2915E−4	3.7474E−2
64	1.5844E−4	3.5334E−2	6.2281E−3	5.7279E−5	1.8738E−2
Rate	1.9891	0.9864	1.2263	1.9972	0.9994

where p_K is the restrict of p_h on element $K \in \mathcal{T}_{h_f}$ and $V_j(K)$ is the volume of the element $K \in S_j$. See [79] for more details about the construction of Π_h^1. Hence it is easy to see that $I - \Pi_h^1$ can be explicitly computed at the element level. And the stabilization term can be computed by $\forall K \in \mathcal{T}_{h_f}, \forall p_h,\ q_h \in Q_{h_f}^0$

$$G(p_h, q_h) = \sum_{K \in \mathcal{T}_{h_f}} \left((p_h, q_h)_K - (\sum_{p_j \in K} w_j \phi_j, q_h)_K - (p_h, \sum_{p_j \in K} w_j \phi_j)_K + (\sum_{p_j \in K} w_j \phi_j, \sum_{p_j \in K} w_j \phi_j)_K \right). \tag{57}$$

Example 1. We first investigate on the solution errors and convergence rates of the proposed method with different implementation techniques by using this example with known analytic solutions. Let the computational domain be $\Omega = [0,1] \times [-1,1]$, where $\Omega_f = [0,1] \times [0,1]$, $\Omega_p = [0,1] \times [-1,0]$, and $\Gamma = [0,1] \times \{0\}$. Choose $\frac{\alpha \nu \sqrt{d}}{\sqrt{trace(\mathbf{\Pi})}} = 1$, $\nu = 1$, $g = 1$, $z = 0$, and $\mathbb{K} = k\mathbb{I}$, where $\mathbb{I}$ is the identity matrix and $k = 1$. The Dirichlet boundary data and the source terms are chosen such that the exact solution of the Stokes–Darcy system with the Beavers–Joseph–Saffman–Jones interface boundary condition is given by

$$\begin{cases} \phi_p = (e^y - e^{-y}) \sin(x), \\ \mathbf{u}_f = [\frac{k}{\pi} \sin(2\pi y) \cos(x), (-2k + \frac{k}{\pi^2} (\sin(\pi y))^2) \sin(x)]^T, \\ p_f = 0. \end{cases} \tag{58}$$

In Tables 1–3, we provide the solution errors in both L^2 and H^1 norms for the two finite element triples: P_1–P_0–P_1 and P_1–P_1–P_1. Both the implicit implementation and the explicit implementation are considered for the stabilization term. These errors demonstrate the optimal convergence rates obtained in Theorem 4.3.2.

For the finite element triples P_1–P_0–P_1, the results of the explicit implementation of the stabilization term in Table 1 are optimal and very close to those of the implicit implementation in Table 2, which numerically validates the convenient explicit implementation technique. For the finite element triples P_1–P_1–P_1, the results of the implicit implementation of the stabilization term are the same as those of the explicit implementation in Table 3. This agrees with the theoretical equivalence between the two types of implementation. We omit the redundant data here in order to shorten the presentation. Since the explicit implementation is more convenient than the implicit one while reaching the same optimal accuracy, it is natural in practice to utilize the explicit implementation.

Example 2. We consider a numerical example in [51] to present our computational results of mass conservation and robustness with respect to the permeability for the proposed finite volume element method. Let the computational domain be $\Omega = [0,2] \times [0,2]$, where $\Omega_f = [0,1] \times [0,2]$, $\Omega_p = [1,2] \times [0,2]$, and $\Gamma = \{1\} \times [0,2]$. The Ω_f is the free-flow domain with a quadratic inflow profile $\mathbf{u}_f = [y(2-y), 0]$ on the left boundary and no-slip boundary conditions $\mathbf{u}_f = [0,0]$ on the top and bottom boundaries. For the Darcy domain Ω_p, Neumann boundary condition $\nabla \phi_p \cdot \mathbf{n} = 0$ is imposed on the top and bottom boundary and Dirichlet boundary condition $\phi_p = 0$ is imposed on the right boundary. Choose $\frac{\alpha \nu \sqrt{d}}{\sqrt{trace(\mathbf{\Pi})}} = 1$, $\nu = 1$, $g = 1$, $z = 0$, and $\mathbb{K} = k\mathbb{I}$. Let $\mathbf{f}_f = \mathbf{0}$ in Ω_f and $f_p = 0$ in Ω_p. To quantify the local mass-conservation characteristics,

Table 3
Errors of the P_1–P_1–P_1 with explicit (implicit) implementation of the stabilization term.

$\frac{1}{h}$	$\|\mathbf{u}_f - \mathbf{u}_f{}^h\|_0$	$\|\mathbf{u}_f - \mathbf{u}_f{}^h\|_1$	$\|p - p_h\|_0$	$\|\phi_p - \phi_p{}^h\|_0$	$\|\phi_p - \phi_p{}^h\|_1$
4	3.8762E−2	5.4534E−1	1.3795E−1	1.4550E−2	2.9927E−1
8	9.9243E−3	2.8036E−1	5.2526E−2	3.6610E−3	1.4983E−1
16	2.4877E−3	1.4109E−1	1.5774E−2	9.1642E−4	7.4942E−2
32	6.2193E−4	7.0646E−2	4.5826E−3	2.2912E−4	3.7474E−2
64	1.5548E−4	3.5334E−2	1.3725E−3	5.7272E−5	1.8738E−2
Rate	1.9905	0.9871	1.6710	1.9972	0.9994

Table 4
The mass errors of the P_1–P_1–P_1 with different k in Example 2.

$\frac{1}{h}$	$k = 1$	$k = 10^{-2}$	$k = 10^{-4}$	$k = 10^{-6}$
4	2.4351E−2	2.2135E−2	2.1228E−2	2.1211E−2
8	5.8995E−3	5.4333E−3	5.2191E−3	5.2140E−3
16	1.4502E−3	1.3577E−3	1.3041E−3	1.3022E−3
32	3.5768E−4	3.3967E−4	3.2628E−4	3.2553E−4
64	8.8332E−5	8.4834E−5	8.1651E−5	8.1385E−5

we consider the finite element triples P_1–P_1–P_1 with the explicit implementation of the stabilization term. The boundary conditions on top and bottom sides of the whole domain imply that there is no mass lost there. So we intend to use the difference of integrals of normal flux between left and right sides, namely inflow and out flow sides, to illustrate the mass conservation of stabilized FVE method, we define the mass balance based on definition in [26] with slight modifications, let

$$\theta = |\int_{\Gamma_{in}} \mathbf{u}_h^* \cdot \mathbf{n}_{in} ds + \int_{\Gamma_{out}} \mathbb{K}\nabla\phi_h^* \cdot \mathbf{n}_{out} ds|,$$

where Γ_{in} and Γ_{out} are inflow and out flow sides respectively, and $\mathbf{n}_{in}$ and $\mathbf{n}_{out}$ are the corresponding exterior unit normal vector of Γ_{in} and Γ_{out}. It's easy to compute the incoming flux integral equal to $\frac{4}{3}$. After a numerical piezometric head ϕ_h^* is obtained, then a numerical normal flux $-\mathbb{K}\nabla\phi_h^* \cdot \mathbf{n}$ on the right boundary is computed. In Table 4, we show θ with different $k = 1, 10^{-2}, 10^{-4}, 10^{-6}$ and $h = 1/4, 1/8, 1/16, 1/32, 1/64$. It is easy to observe that θ converges to 0 for all k with the optimal rate $O(h^2)$, which well illustrates the mass conservation and the robustness of the method with respect to k. Second, set $h = 1/64$ for the uniform mesh, we show the speed and the velocity streamlines for $k = 1, 10^{-2}, 10^{-4}, 10^{-6}$ in Fig. 4, where the warmer color indicates higher speed of the flow.

Example 3. In this test we are interested in the application of the Stokes–Darcy model and the proposed method to an industrial filtration system with curved boundaries [26,44].

The computational domain is a circular sector divided into the porous media and free flow sub-domains as shown in Fig. 5. We impose homogeneous Dirichlet boundary condition on Γ_{p2} and homogeneous Neumann boundary condition on Γ_{p1} and Γ_{p3}. On the boundary of the free flow sub-domain, we impose the following Dirichlet boundary condition.

$$\mathbf{u}_f = \begin{cases} (-x/30, -y/30)^T, \text{ on } \Gamma_{f1}, \\ (0, -0.1)^T, \text{ on } \Gamma_{f2}, \\ (-0.1, 0)^T, \text{ on } \Gamma_{f3}. \end{cases} \tag{59}$$

Choose $\alpha = 0.1$, $\nu = 1$, $g = 1$, $z = 0$, and $\mathbb{K} = k\mathbb{I}$. Set $\mathbf{f}_f = \mathbf{0}$ in Ω_f, $f_p = 0$ in Ω_p. We divide Ω into 45542 triangular elements, with 17356 elements for Stokes domain and 28186 elements for Darcy domain. Consider the finite element triples P_1–P_1–P_1 with the explicit implementation of the stabilization term.

First, we consider the permeability in the porous medium is equal to 10^{-6}. Fig. 6(a) shows the speed and the streamlines of the velocity and Fig. 6(b) shows the pressure. Second, we test the lower porous medium permeability, which is equal to 10^{-11}. Fig. 7(a) shows the speed and the streamlines of the velocity and Fig. 7(b) shows the pressure. As we can see in Figs. 6(b) and 7(b), the lower permeability in the porous medium results in a build up of pressure. The above results are consistent with those obtained in [26].

To accurately simulating a filtration process, mass conservation is another critical property of the utilized numerical model. For the above two cases with $k = 10^{-6}$ and $k = 10^{-11}$, we give the mass balance $\theta = 9.6E{-}3$ and $9.6E{-}3$ respectively, which clearly illustrate the capability of the proposed method to keep the mass conservation.

Example 4. In the last example, we apply the proposed method to a more realistic simulation of the subsurface flow in a karst aquifer. As shown in Fig. 8(left), the computational domain is a unit square divided into the porous media domain

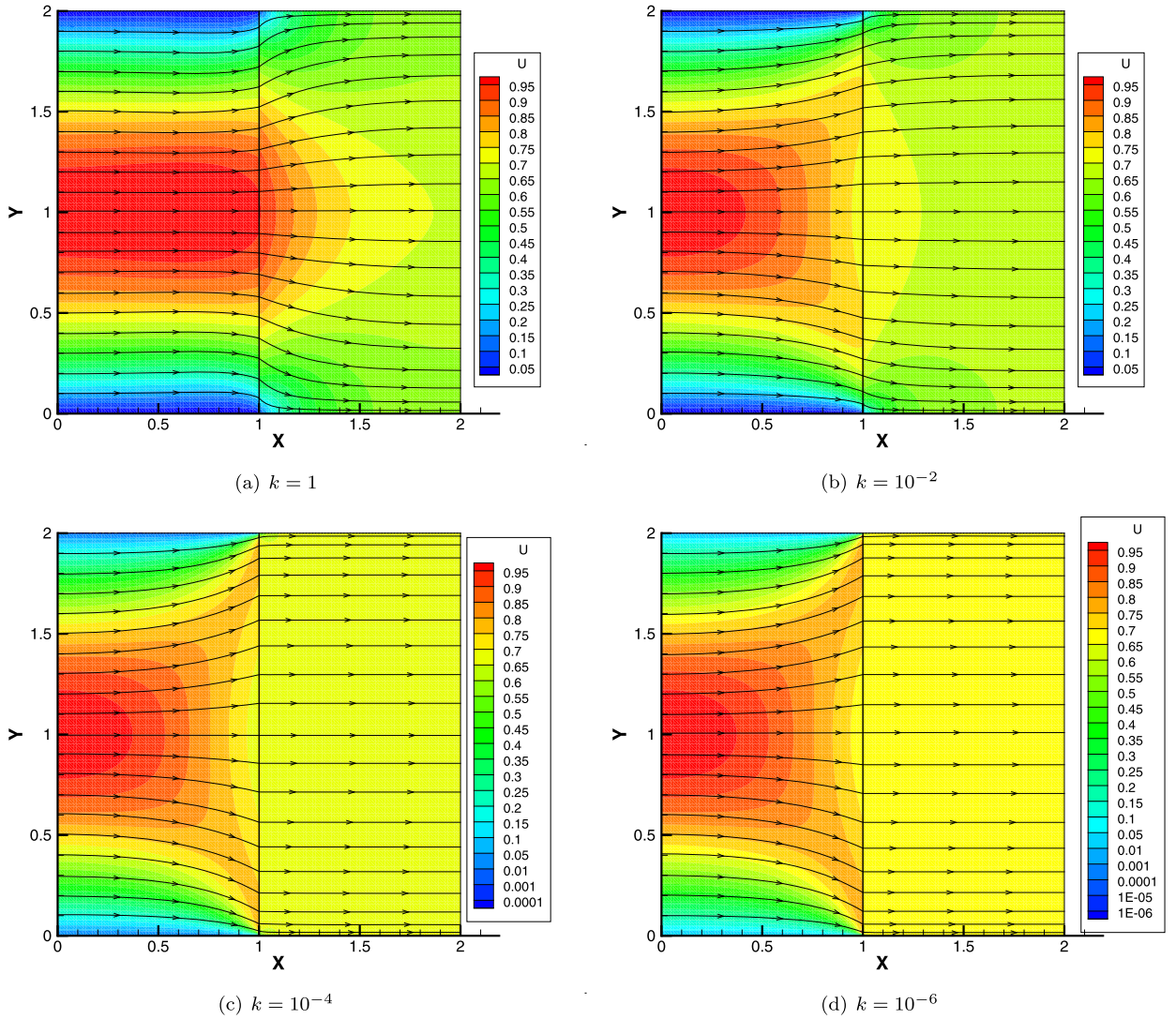

(a) $k = 1$ (b) $k = 10^{-2}$

(c) $k = 10^{-4}$ (d) $k = 10^{-6}$

Fig. 4. Plot of the speed and the velocity streamlines for different k in Example 2. (For interpretation of the references to color in this figure, the reader is referred to the web version of this article.)

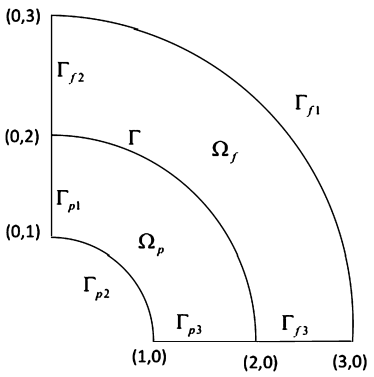

Fig. 5. Computational domain of a filtration problem.

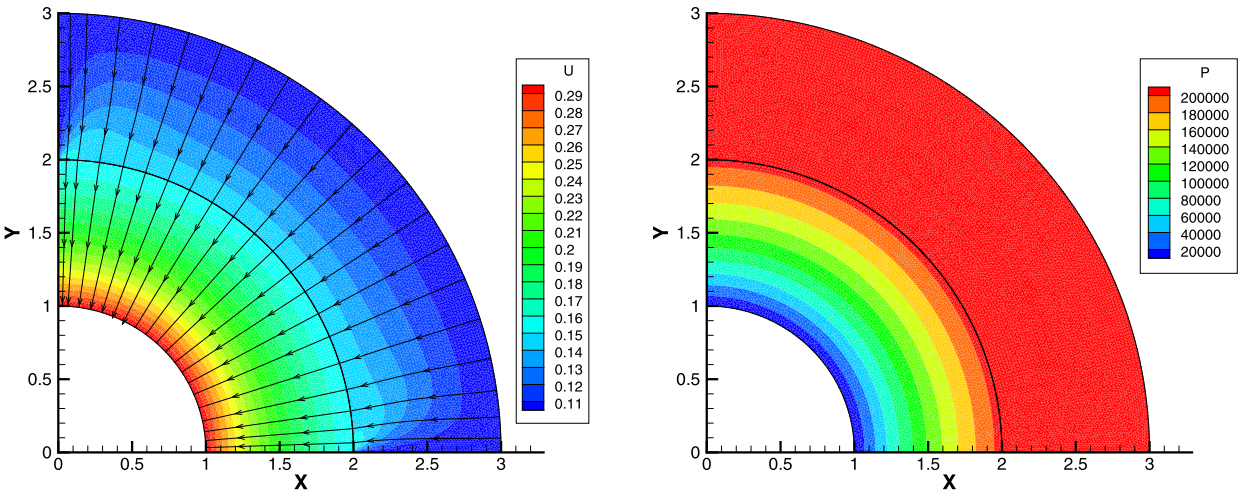

(a) Streamlines and velocity. (b) Pressure.

Fig. 6. P_1–P_1–P_1 with explicit implementation of the stabilization term for dead-end filter with $K = 10^{-6}$. (For interpretation of the references to color in this figure, the reader is referred to the web version of this article.)

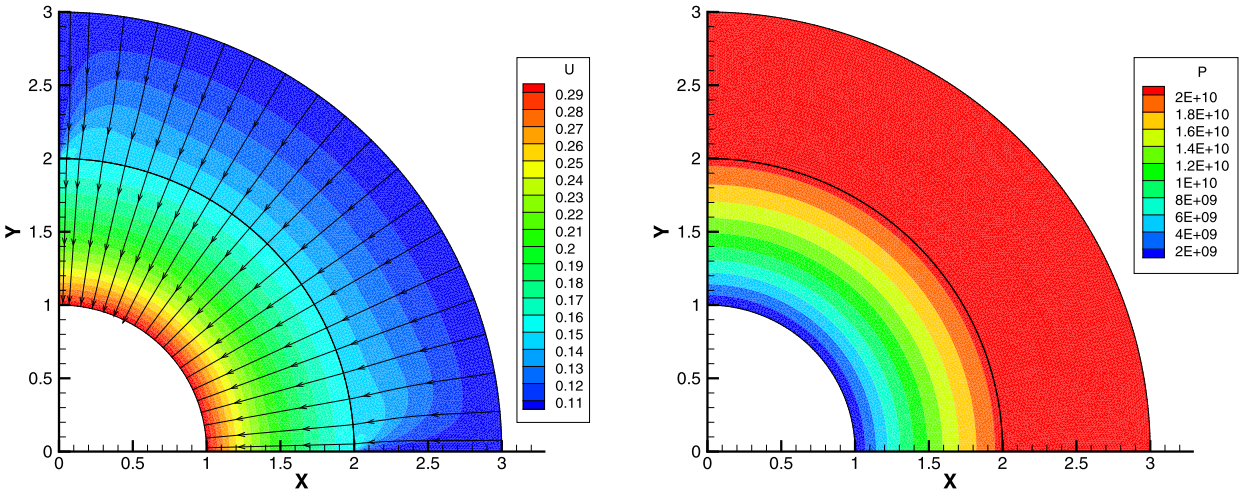

(a) Streamlines and velocity. (b) Pressure.

Fig. 7. P_1–P_1–P_1 with explicit implementation of the stabilization term for dead-end filter with $K = 10^{-11}$. (For interpretation of the references to color in this figure, the reader is referred to the web version of this article.)

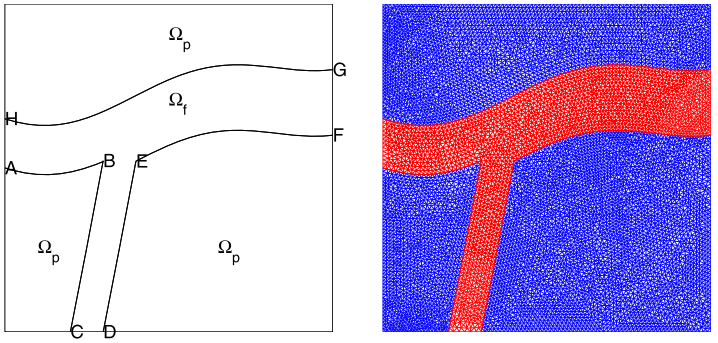

Fig. 8. Computational domain of a model problem. (For interpretation of the references to color in this figure, the reader is referred to the web version of this article.)

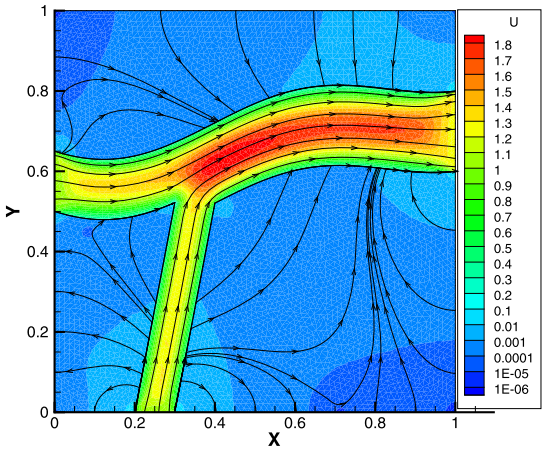

(a) $s_1 = 1, s_2 = 1.25, k = 10^{-6}$.

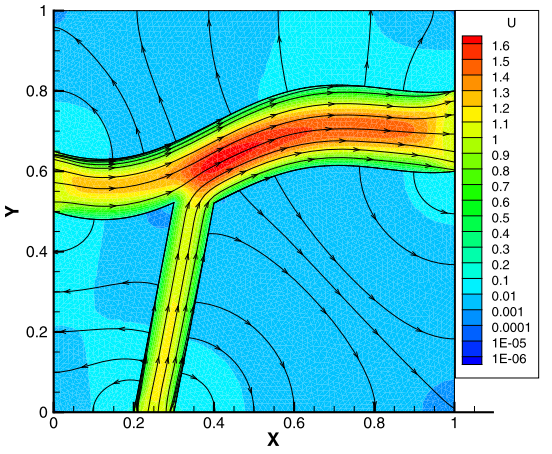

(b) $s_1 = 1, s_2 = 1.0, k = 10^{-6}$.

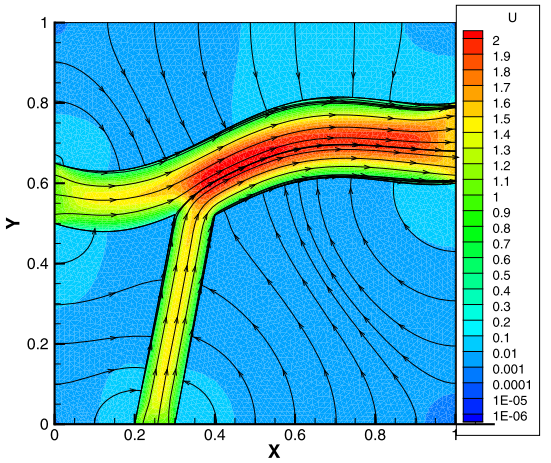

(c) $s_1 = 1, s_2 = 1.5, k = 10^{-6}$.

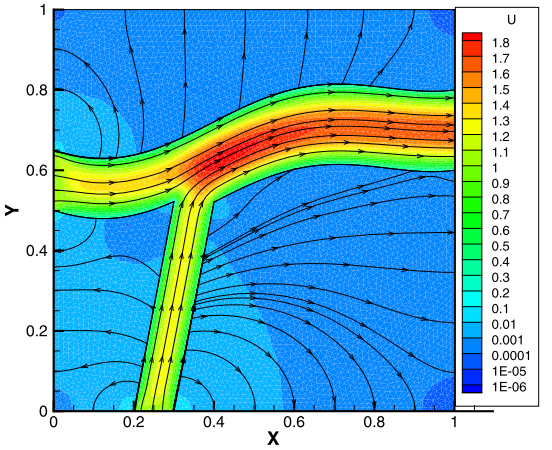

(d) $s_1 = 1, k = 10^{-6}$.

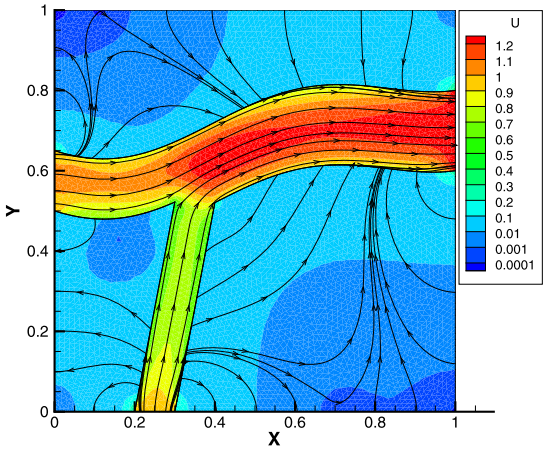

(e) $s_1 = 1, s_2 = 1.25, k = 10^{-4}$.

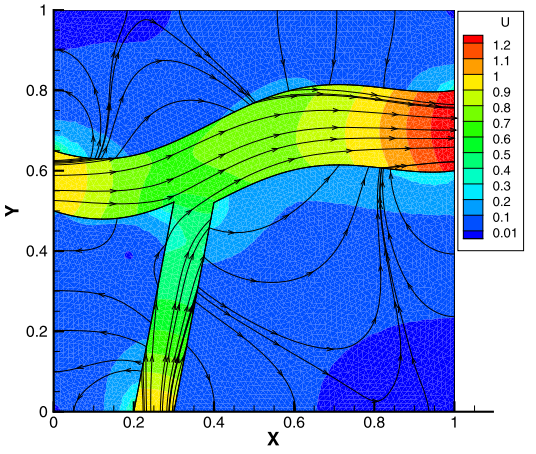

(f) $s_1 = 1, s_2 = 1.25, k = 10^{-2}$.

Fig. 9. Streamlines and velocity for P_1–P_1–P_1 with explicit implementation of the stabilization term. (For interpretation of the references to color in this figure, the reader is referred to the web version of this article.)

Ω_p and the free flow domain Ω_f. Let Ω_f be the bounded curved domain $ABCDEFGH$ with $A=(0,0.5)$, $B=(0.3,0.5219)$, $C=(0.2,0)$, $D=(0.3,0)$, $E=(0.4,0.5207)$, $F=(1,0.6)$, $G=(1,0.8)$, and $H=(0,0.65)$, $\Omega_p=\Omega/\Omega_f$. Let $\Gamma=\overline{\Omega}_f\bigcap\overline{\Omega}_p$. Compared with the Y-shape conduit in [45], we particularly consider the curved interface here. Choose $\alpha=0.1$, $\nu=1$, $g=1$, $z=0$, and $\mathbb{K}=k\mathbb{I}$. Set $\mathbf{f}_f=\mathbf{0}$ in Ω_f, $f_p=0$ in Ω_p, and $\phi_p=0$ in $\partial\Omega_p/\Gamma$. Let

$$\mathbf{u}_f=\begin{cases}(s_1,0)^T, \text{ on } \overline{HA},\\ (0,s_1)^T, \text{ on } \overline{CD},\\ (s_2,0)^T, \text{ on } \overline{FG}.\end{cases} \tag{60}$$

where s_1 and s_2 are two constants. As shown in Fig. 8(right), we divide Ω into 17842 triangular elements: 3934 elements for Stokes domain and 13908 elements for Darcy domain.

In the following, consider the finite element triples P_1–P_1–P_1 with the explicit implementation of the stabilization term. We will first discuss the effect of different inflow and outflow rates. In Fig. 9, the warmer color indicates higher speed of the flow and the line with arrows is the streamline. We choose $s_1=1$ and $s_2=1.25$ in Fig. 9(a), $s_1=1$ and $s_2=1$ in Fig. 9(b), and $s_1=1$ and $s_2=1.5$ in Fig. 9(c). Compared with 9(a), we can see that (1) the less outflow rate in Fig. 9(b) causes more water to be pushed out of the conduits into the porous media, which is what happens during a rain season; (2) the more outflow rate in Fig. 9(c) causes more water to flow into the conduits from the porous media, which is what happens during a dry season.

Furthermore, we show the effect of different boundary conditions by comparing Fig. 9(b) with Fig. 9(d). Let

$$\mathbf{u}_f=\begin{cases}(s_1,0)^T, \text{ on } \overline{HA},\\ (0,s_1)^T, \text{ on } \overline{CD},\end{cases} \tag{61}$$

and we impose the free outflow boundary conditions for the Stokes flow velocity on $\overline{FG}$. Choose $s_1=1$ and $k=10^{-6}$. The simulation results are showed in Fig. 9(d). Compared with Fig. 9(b), the free outflow boundary condition increases the flow speed in the conduits and hence changes the flow performance in the porous media.

Finally, we test the effect of k on the solution. Figs. 9(e) and 9(f) show the simulation results for $k=10^{-4},10^{-2}$ with $s_1=1$ and $s_2=1.25$. When k becomes smaller, the flow speed in porous media is significantly reduced.

6. Conclusions

A stabilized finite volume element method was proposed to solve the coupled Stokes–Darcy model with two conforming finite element triples. Rigorous error estimates are proved through an equivalence between the stabilized finite volume element method and the stabilized finite element method. Implementation techniques for the stabilization are discussed. Four numerical examples were presented to show that this convenient and efficient method with mass conservation is optimally convergent, robust, and applicable for the realistic problems of coupling free and porous media flow.

References

[1] T. Arbogast, M. Gomez, A discretization and multigrid solver for a Darcy–Stokes system of three dimensional vuggy porous media, Comput. Geosci. 13 (3) (2009) 331–348.
[2] T. Arbogast, H.L. Lehr, Homogenization of a Darcy–Stokes system modeling vuggy porous media, Comput. Geosci. 10 (3) (2006) 291–302.
[3] I. Babuška, G.N. Gatica, A residual-based a posteriori error estimator for the Stokes–Darcy coupled problem, SIAM J. Numer. Anal. 48 (2) (2010) 498–523.
[4] G. Beavers, D. Joseph, Boundary conditions at a naturally permeable wall, J. Fluid Mech. 30 (1967) 197–207.
[5] C. Bi, C. Wang, A posteriori error estimates of finite volume element method for second-order quasilinear elliptic problems, Int. J. Numer. Anal. Model. 13 (1) (2016) 22–40.
[6] P. Bochev, C. Dohrmann, M.D. Gunzburger, Stabilization of low-order mixed finite elements for the Stokes equations, SIAM J. Numer. Anal. 44 (1) (2006) 82–101.
[7] Y. Boubendir, S. Tlupova, Stokes–Darcy boundary integral solutions using preconditioners, J. Comput. Phys. 228 (23) (2009) 8627–8641.
[8] Y. Boubendir, S. Tlupova, Domain decomposition methods for solving Stokes–Darcy problems with boundary integrals, SIAM J. Sci. Comput. 35 (1) (2013) B82–B106.
[9] Z. Cai, S. McCormick, On the accuracy of the finite volume element method for diffusion equations on composite grids, SIAM J. Numer. Anal. 27 (3) (1990) 636–655.
[10] Z. Cai, J. Mandel, S. McCormick, The finite volume element method for diffusion equations on general triangulations, SIAM J. Numer. Anal. 28 (2) (1991) 392–402.
[11] M. Cai, M. Mu, J. Xu, Numerical solution to a mixed Navier–Stokes/Darcy model by the two-grid approach, SIAM J. Numer. Anal. 47 (5) (2009) 3325–3338.
[12] J. Camano, G.N. Gatica, R. Oyarzua, R. Ruiz-Baier, P. Venegas, New fully-mixed finite element methods for the Stokes–Darcy coupling, Comput. Methods Appl. Mech. Eng. 295 (2015) 362–395.
[13] Y. Cao, M. Gunzburger, X. Hu, F. Hua, X. Wang, W. Zhao, Finite element approximation for Stokes–Darcy flow with Beavers–Joseph interface conditions, SIAM J. Numer. Anal. 47 (6) (2010) 4239–4256.
[14] Y. Cao, M. Gunzburger, F. Hua, X. Wang, Coupled Stokes–Darcy model with Beavers–Joseph interface boundary condition, Commun. Math. Sci. 8 (1) (2010) 1–25.
[15] Y. Cao, M. Gunzburger, X.-M. He, X. Wang, Robin–Robin domain decomposition methods for the steady Stokes–Darcy model with Beaver–Joseph interface condition, Numer. Math. 117 (4) (2011) 601–629.

[16] Y. Cao, Y. Chu, X.-M. He, M. Wei, Decoupling the stationary Navier–Stokes–Darcy system with the Beavers–Joseph–Saffman interface condition, Abstr. Appl. Anal. (2013) 136483.
[17] Y. Cao, M. Gunzburger, X.-M. He, X. Wang, Parallel, non-iterative, multi-physics domain decomposition methods for time-dependent Stokes–Darcy systems, Math. Comput. 83 (288) (2014) 1617–1644.
[18] A. Çeşmelioğlu, B. Rivière, Primal discontinuous Galerkin methods for time-dependent coupled surface and subsurface flow, J. Sci. Comput. 40 (1–3) (2009) 115–140.
[19] P. Chatzipantelidis, R.D. Lazarov, V. Thomée, Error estimates for a finite volume element method for parabolic equations in convex polygonal domains, Numer. Methods Partial Differ. Equ. 20 (5) (2004) 650–674.
[20] P. Chatzipantelidis, V. Ginting, R.D. Lazarov, A finite volume element method for a non-linear elliptic problem, Numer. Linear Algebra Appl. 12 (5–6) (2005) 515–546.
[21] Z. Chen, Finite Element Methods and Their Applications, Scientific Computation, Springer-Verlag, Berlin, 2005.
[22] L. Chen, A new class of high order finite volume methods for second order elliptic equations, SIAM J. Numer. Anal. 47 (6) (2010) 4021–4043.
[23] Z. Chen, Y. Xu, Y. Zhang, A construction of higher-order finite volume methods, Math. Comput. 84 (292) (2015) 599–628.
[24] W. Chen, F. Wang, Y. Wang, Weak Galerkin method for the coupled Darcy–Stokes flow, IMA J. Numer. Anal. 36 (2) (2016) 897–921.
[25] Z. Chen, Y. Xu, J. Zhang, A second-order hybrid finite volume method for solving the Stokes equation, Appl. Numer. Math. 119 (2017) 213–224.
[26] P. Chidyagwai, B. Riviére, Numerical modelling of coupled surface and subsurface flow systems, Adv. Water Resour. 33 (2010) 92–105.
[27] M. Cui, X. Ye, Unified analysis of finite volume methods for the Stokes equations, SIAM J. Numer. Anal. 48 (3) (2010) 824–839.
[28] M. Discacciati, Domain Decomposition Methods for the Coupling of Surface and Groundwater Flows, PhD thesis, Ecole Polytechnique Fédérale de Lausanne, Switzerland, 2004.
[29] M. Discacciati, A. Quarteroni, Convergence analysis of a subdomain iterative method for the finite element approximation of the coupling of Stokes and Darcy equations, Comput. Vis. Sci. 6 (2–3) (2004) 93–103.
[30] M. Discacciati, E. Miglio, A. Quarteroni, Mathematical and numerical models for coupling surface and groundwater flows, Appl. Numer. Math. 43 (1–2) (2002) 57–74.
[31] M. Discacciati, A. Quarteroni, A. Valli, Robin–Robin domain decomposition methods for the Stokes–Darcy coupling, SIAM J. Numer. Anal. 45 (3) (2007) 1246–1268.
[32] V.J. Ervin, E.W. Jenkins, S. Sun, Coupling nonlinear Stokes and Darcy flow using mortar finite elements, Appl. Numer. Math. 61 (11) (2011) 1198–1222.
[33] V.J. Ervin, E.W. Jenkins, H. Lee, Approximation of the Stokes–Darcy system by optimization, J. Sci. Comput. 59 (3) (2014) 775–794.
[34] W. Feng, X.-M. He, Z. Wang, X. Zhang, Non-iterative domain decomposition methods for a non-stationary Stokes–Darcy model with Beavers–Joseph interface condition, Appl. Math. Comput. 219 (2) (2012) 453–463.
[35] J. Galvis, M. Sarkis, Non-matching mortar discretization analysis for the coupling Stokes–Darcy equations, Electron. Trans. Numer. Anal. 26 (2007) 350–384.
[36] Gabriel N. Gatica, Filánder A. Sequeira, Analysis of the HDG method for the Stokes–Darcy coupling, Numer. Methods Partial Differ. Equ. 33 (3) (2017) 885–917.
[37] G.N. Gatica, S. Meddahi, R. Oyarzúa, A conforming mixed finite-element method for the coupling of fluid flow with porous media flow, IMA J. Numer. Anal. 29 (1) (2009) 86–108.
[38] G.N. Gatica, R. Oyarzúa, F.J. Sayas, A residual-based a posteriori error estimator for a fully-mixed formulation of the Stokes–Darcy coupled problem, Comput. Methods Appl. Mech. Eng. 200 (21–22) (2011) 1877–1891.
[39] V. Girault, P.A. Raviart, Finite Element Methods for Navier–Stokes Equations: Theory and Algorithms, Springer Ser. Comput. Math., vol. 5, Springer-Verlag, Berlin, 1986.
[40] V. Girault, B. Rivière, DG approximation of coupled Navier–Stokes and Darcy equations by Beaver–Joseph–Saffman interface condition, SIAM J. Numer. Anal. 47 (3) (2009) 2052–2089.
[41] V. Girault, D. Vassilev, I. Yotov, Mortar multiscale finite element methods for Stokes–Darcy flows, Numer. Math. 127 (1) (2014) 93–165.
[42] M. Gunzburger, Finite Element Methods for Viscous Incompressible Flows: A Guide to Theory, Practice, and Algorithms, Computer Science and Scientific Computing, Academic Press, Boston, MA, 1989.
[43] M. Gunzburger, X.-M. He, B. Li, On Ritz projection and multi-step backward differentiation schemes in decoupling the Stokes–Darcy model, SIAM J. Numer. Anal. (2017), accepted.
[44] N. Hanspal, A. Waghode, V. Nassehi, R. Wakeman, Numerical analysis of coupled Stokes/Darcy flow in industrial filtrations, Transp. Porous Media 64 (2006) 73–101.
[45] X.-M. He, J. Li, Y. Lin, J. Ming, A domain decomposition method for the steady-state Navier–Stokes–Darcy model with Beavers–Joseph interface condition, SIAM J. Sci. Comput. 37 (5) (2015) S264–S290.
[46] P. Hessari, Pseudospectral least squares method for Stokes–Darcy equations, SIAM J. Numer. Anal. 53 (3) (2015) 1195–1213.
[47] R. Hoppe, P. Porta, Y. Vassilevski, Computational issues related to iterative coupling of subsurface and channel flows, Calcolo 44 (1) (2007) 1–20.
[48] J. Hou, X.-M. He, C. Guo, M. Wei, B. Bai, A dual-porosity-Stokes model and finite element method for coupling dual-porosity flow and free flow, SIAM J. Sci. Comput. 38 (5) (2016) B710–B739.
[49] G. Jin, H. Li, Q. Zhang, Q. Zou, Linear and quadratic finite volume methods on triangular meshes for elliptic equations with singular solutions, Int. J. Numer. Anal. Model. 13 (2) (2016) 240–260.
[50] I. Jones, Low Reynolds number flow past a porous spherical shell, Proc. Camb. Philos. Soc. 73 (1973) 231–238.
[51] G. Kanschat, B. Riviére, A strongly conservative finite element method for the coupling of Stokes and Darcy flow, J. Comput. Phys. 229 (2010) 5933–5943.
[52] T. Karper, K.A. Mardal, R. Winther, Unified finite element discretizations of coupled Darcy–Stokes flow, Numer. Methods Partial Differ. Equ. 25 (2) (2009) 311–326.
[53] M. Kubacki, M. Moraiti, Analysis of a second-order, unconditionally stable, partitioned method for the evolutionary Stokes–Darcy model, Int. J. Numer. Anal. Model. 12 (4) (2015) 704–730.
[54] W.J. Layton, F. Schieweck, I. Yotov, Coupling fluid flow with porous media flow, SIAM J. Numer. Anal. 40 (6) (2002) 2195–2218.
[55] W. Layton, H. Tran, C. Trenchea, Analysis of long time stability and errors of two partitioned methods for uncoupling evolutionary groundwater-surface water flows, SIAM J. Numer. Anal. 51 (1) (2013) 248–272.
[56] H. Lee, K. Rife, Least squares approach for the time-dependent nonlinear Stokes–Darcy flow, Comput. Math. Appl. 67 (10) (2014) 1806–1815.
[57] J. Li, Z. Chen, A new stabilized finite volume method for the stationary Stokes equations, Adv. Comput. Math. 30 (2) (2009) 141–152.
[58] R. Li, J. Li, Z. Chen, Y. Gao, A stabilized finite element method based on two local Gauss integrations for a coupled Stokes–Darcy problem, J. Comput. Appl. Math. 292 (2016) 92–104.
[59] R. Li, Y. Gao, J. Li, Z. Chen, Discontinuous finite volume element method for a coupled non-stationary Stokes–Darcy problem, J. Sci. Comput. (2017), http://dx.doi.org/10.1007/s10915-017-0454-3.
[60] R. Li, J. Li, X. Liu, Z. Chen, A weak Galerkin finite element method for a coupled Stokes–Darcy problem, Numer. Methods Partial Differ. Equ. 33 (4) (2017) 1352–1373.

[61] K. Lipnikov, D. Vassilev, I. Yotov, Discontinuous Galerkin and mimetic finite difference methods for coupled Stokes–Darcy flows on polygonal and polyhedral grids, Numer. Math. 126 (2) (2014) 321–360.
[62] A. Márquez, S. Meddahi, F.J. Sayas, Strong coupling of finite element methods for the Stokes–Darcy problem, IMA J. Numer. Anal. 35 (2) (2015) 969–988.
[63] I.D. Mishev, Finite volume element methods for non-definite problems, Numer. Math. 83 (1) (1999) 161–175.
[64] M. Mu, J. Xu, A two-grid method of a mixed Stokes–Darcy model for coupling fluid flow with porous media flow, SIAM J. Numer. Anal. 45 (5) (2007) 1801–1813.
[65] M. Mu, X. Zhu, Decoupled schemes for a non-stationary mixed Stokes–Darcy model, Math. Comput. 79 (270) (2010) 707–731.
[66] S. Münzenmaier, G. Starke, First-order system least squares for coupled Stokes–Darcy flow, SIAM J. Numer. Anal. 49 (1) (2011) 387–404.
[67] B. Rivière, Analysis of a discontinuous finite element method for the coupled Stokes and Darcy problems, J. Sci. Comput. 22 (23) (2005) 479–500.
[68] B. Rivière, I. Yotov, Locally conservative coupling of Stokes and Darcy flows, SIAM J. Numer. Anal. 42 (5) (2005) 1959–1977.
[69] P. Saffman, On the boundary condition at the interface of a porous medium, Stud. Appl. Math. 1 (1971) 77–84.
[70] L. Shan, H. Zheng, Partitioned time stepping method for fully evolutionary Stokes–Darcy flow with Beavers–Joseph interface conditions, SIAM J. Numer. Anal. 51 (2) (2013) 813–839.
[71] S. Tlupova, R. Cortez, Boundary integral solutions of coupled Stokes and Darcy flows, J. Comput. Phys. 228 (1) (2009) 158–179.
[72] J.M. Urquiza, D. N'Dri, A. Garon, M.C. Delfour, Coupling Stokes and Darcy equations, Appl. Numer. Math. 58 (5) (2008) 525–538.
[73] D. Vassilev, C. Wang, I. Yotov, Domain decomposition for coupled Stokes and Darcy flows, Comput. Methods Appl. Mech. Eng. 268 (2014) 264–283.
[74] J. Wang, Y. Wang, X. Ye, A new finite volume method for the Stokes problems, Int. J. Numer. Anal. Model. 7 (2) (2010) 281–302.
[75] G. Wang, Y. He, R. Li, Discontinuous finite volume methods for the stationary Stokes–Darcy problem, Int. J. Numer. Methods Eng. 107 (5) (2016) 395–418.
[76] J. Xu, Q. Zou, Analysis of linear and quadratic simplicial finite volume methods for elliptic equations, Numer. Math. 111 (3) (2009) 469–492.
[77] X. Ye, On the relationship between finite volume and finite element methods applied to the Stokes equations, Numer. Methods Partial Differ. Equ. 5 (2001) 440–453.
[78] T. Zhang, L. Tang, A stabilized finite volume method for Stokes equations using the lowest order P_1–P_0 element pair, Adv. Comput. Math. 41 (4) (2015) 781–798.
[79] H. Zheng, Y. Hou, F. Shi, A posteriori error estimates of stabilization of low-order mixed finite elements for incompressible flow, SIAM J. Sci. Comput. 32 (3) (2010) 1346–1360.
[80] L. Zuo, G. Du, A parallel two-grid linearized method for the coupled Navier–Stokes–Darcy problem, Numer. Algorithms (2017), http://dx.doi.org/10.1007/s11075-017-0308-y.